FEASIBILITY STUDY FOR A 60-GHz RADIOMETRIC ARRAY

By Leonard H. Yorinks

January 1969

Prepared under Contract No. NAS 12-149 by:

RCA Defense Electronic Products | Missile and Surface Radar Division, Moorestown, N.J.

Electronics Research Center

NATIONAL AERONAUTICS AND SPACE ADMINISTRATION

Dr. Robert J. Mailloux
Technical Monitor
EMA
Electronics Research Center
575 Technology Square
Cambridge, Massachusetts 02139

Request for copies of this report should be referred to:

NASA Scientific and Technical Information Facility
P. O. Box 33, College Park, Maryland 20740

FEASIBILITY STUDY FOR A 60-GHz RADIOMETRIC ARRAY

By Leonard H. Yorinks

January 1969

Prepared under Contract No. NAS 12-149 by:

Defense Electronic Products | Missile and Surface Radar Division,
Moorestown, N.J.

Electronics Research Center

NATIONAL AERONAUTICS AND SPACE ADMINISTRATION

CONTENTS

ILLUSTRATIONS

ILLUSTRATIONS (Continued)

TABLES

FEASIBILITY STUDY

FOR A 60-GHz RADIOMETRIC ARRAY

By Leonard H. Yorinks

RCA
DEFENSE ELECTRONIC PRODUCTS

SUMMARY

A novel very low sidelobe array of H-plane sectoral-horn radiating elements excited by a completely constrained optical power combiner has been shown to be feasible for radiometric service at a frequency of 16 GHz. The adaptation of this array concept to operation at 60 GHz and the feasibility of such a 60 GHz radiometer array is the subject of this report. Several areas have received specific attention. The 60 GHz array dimensions are derived from the 16 GHz design. The progress of latching ferrite phase shifters operating at 60 GHz is discussed and present developmental efforts are indicated. Array performance considering the effects of random and systematic errors is predicted based on a statistical analysis and on patterns computed including the effects of errors. Finally, some fabrication techniques are discussed to point out some of the possible construction problems associated with such a 60 GHz array.

INTRODUCTION

It is the purpose of this report to describe a design for an array antenna to operate at approximately 60 GHz. The design will be based on techniques developed for a similar array operating at a center frequency of 16 GHz. The array techniques which have been developed at 16 GHz include the use of a completely constrained optical power combiner to effect a transition from the 50 radiating elements to a single output port. Higher order modes are generated in the power combiner to obtain the necessary amplitude taper which yields very low sidelobe array patterns. The radiating elements are large-aperture wide-flare-angle lens-compensated sectoral H-plane waveguide horns. Ferrite phase shifters are inserted between the power combiner and the horn radiators to provide the phase shift required to electronically steer the array pattern. The use of an optical power combiner rather than a TEE or hybrid network results in a great deal less feed network loss as well as a possible weight savings. An array of horn radiators does not have the extremely tight tolerances necessary in a slotted waveguide array or arrays of small radiating elements. This approach should therefore be very effective at 60 GHz.

The details of the theory of the array design and experimental work done at 16 GHz have been reported in Profera (Refs. 1 and 2) and will not be repeated here. The performance of the 60 GHz array will be projected from the findings at 16 GHz and from other considerations.

The report will consist of four sections: physical configuration; latching ferrite phase shifter; expected performance; and, array fabrication techniques. The physical geometry of the 60 GHz array will be derived from that adopted at 16 GHz. The second section will describe progress which has been made with millimeter wave ferrite phase shifters. Performance in the third section of the report will be predicted from theoretical considerations as well as observed performance at 16 GHz. Effects of tolerances in fabrication and tolerances associated with the ferrite phase shifters will be included in the analysis. In the last section various fabrication techniques which have been considered for construction of the 60 GHz array will be described and evaluated.

Throughout the report, problem areas will be pointed out and possible solutions will be proposed. It is the intention of this report to indicate possible problem areas which require further investigation rather than offer solutions to all possible problems.

PHYSICAL CONFIGURATION

The 50 element low-sidelobe array fabricated at 16 GHz consists of six major components. In order of signal path these are: the horn array, which consists of 50 H-plane horn low-sidelobe radiating elements; a phase correcting dielectric lens for each radiating element; the ferrite phase shifters; the power combiner septated waveguide and matching section; the power combiner E-plane horn; and, the dielectric lens for the power combiner horn. The assembly is shown in Figure 1.

The dimensions of the 60 GHz array are based on those of the 16 GHz model. The general design approach will be to directly scale each component from the 16 GHz model to 60 GHz. Changes will then be suggested and the selection of a component design will be made considering these changes. The major criteria for deciding on a particular design will be projected array performance and ease of fabrication.

In this section, all of the components will be treated except for the ferrite phase shifter. The phase shifter will be described separately.

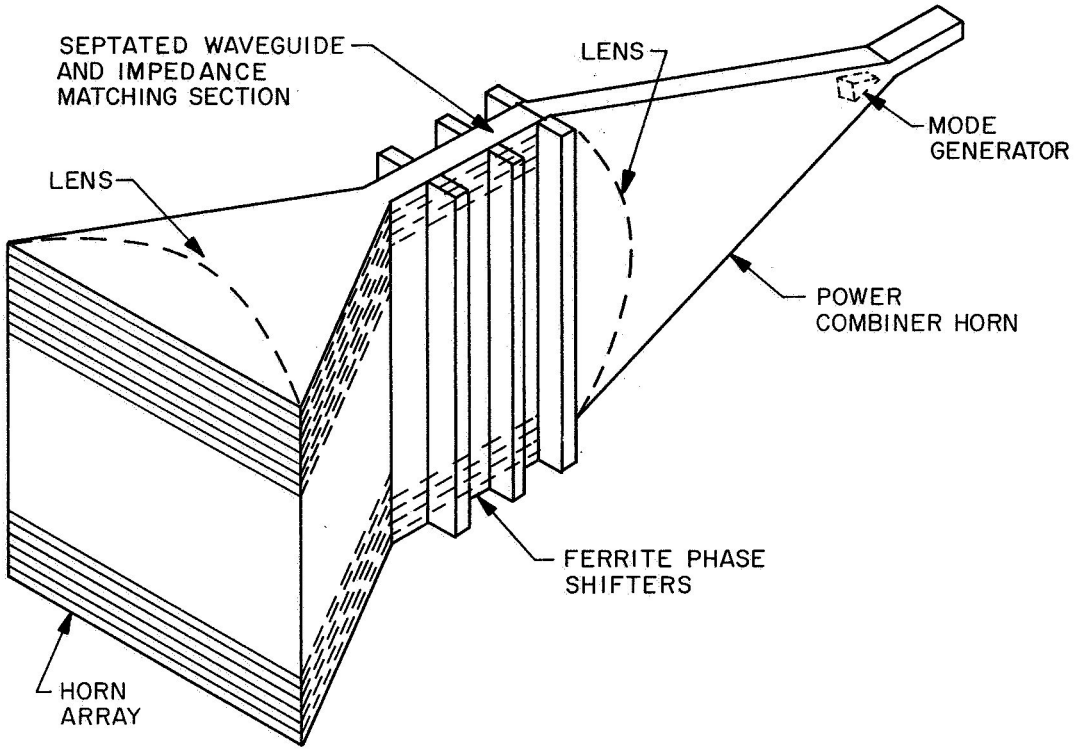

Figure 1. Assembled Array

Horn Array

The horn array consists of 50 H-plane waveguide horns stacked as shown in Figure 2. The dimensions of one of the horns, as obtained by directly scaling the dimensions of the 16 GHz model, are shown in Figure 3. The 0.148 inch input waveguide dimension is a standard waveguide width. The 16 GHz array aperture was chosen to be rectangular to make use of an existing E-plane power combiner developed earlier in the program. Since the power combiner design will be changed, as will be pointed out in a later section, the aperture of the 60 GHz array will be 4.700 inches square. Such an aperture size corresponds to a half-power-beamwidth of 3^{o} at 60 GHz. The final H-plane horn radiating element dimensions are shown in parentheses in Figure 3. The simplicity of the radiating element makes any modifications of the basic design superfluous. The only change necessary allows 50 such horns to occupy 4.7 inches.

Dielectric Lens For Radiating Element

Scaling the phase correcting dielectric lens of the radiating element to 60 GHz gives a lens whose dimensions are shown in Figure 4. It should be noted that the impedance matching ridges are extremely thin and may be extremely fragile. An alternative approach, wherein the impedance match is obtained by corrugating these

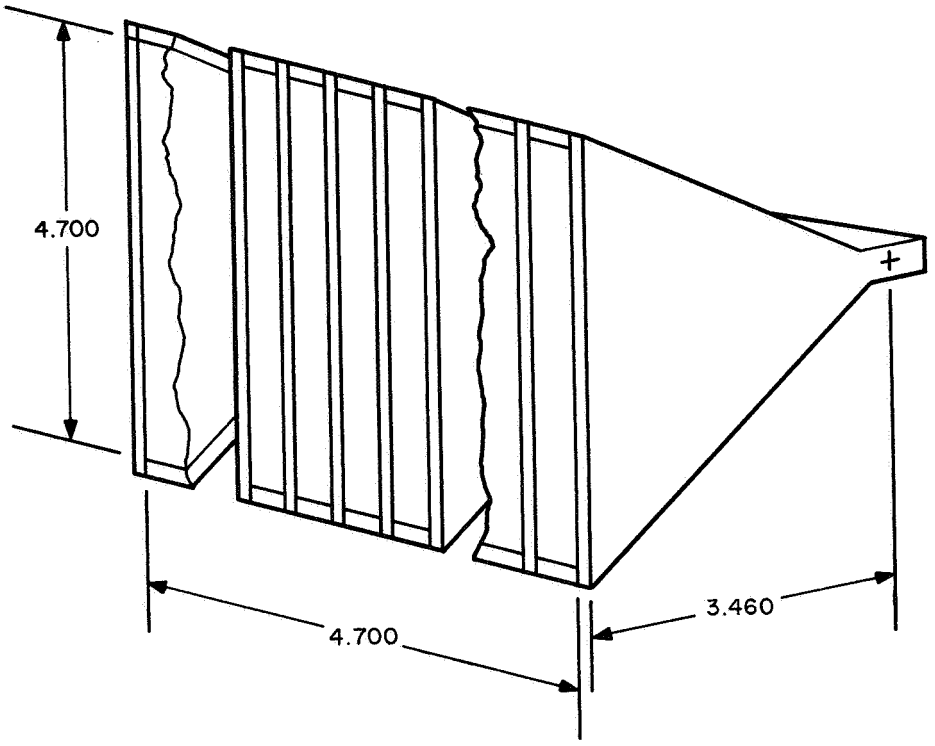

Figure 2. Horn Array

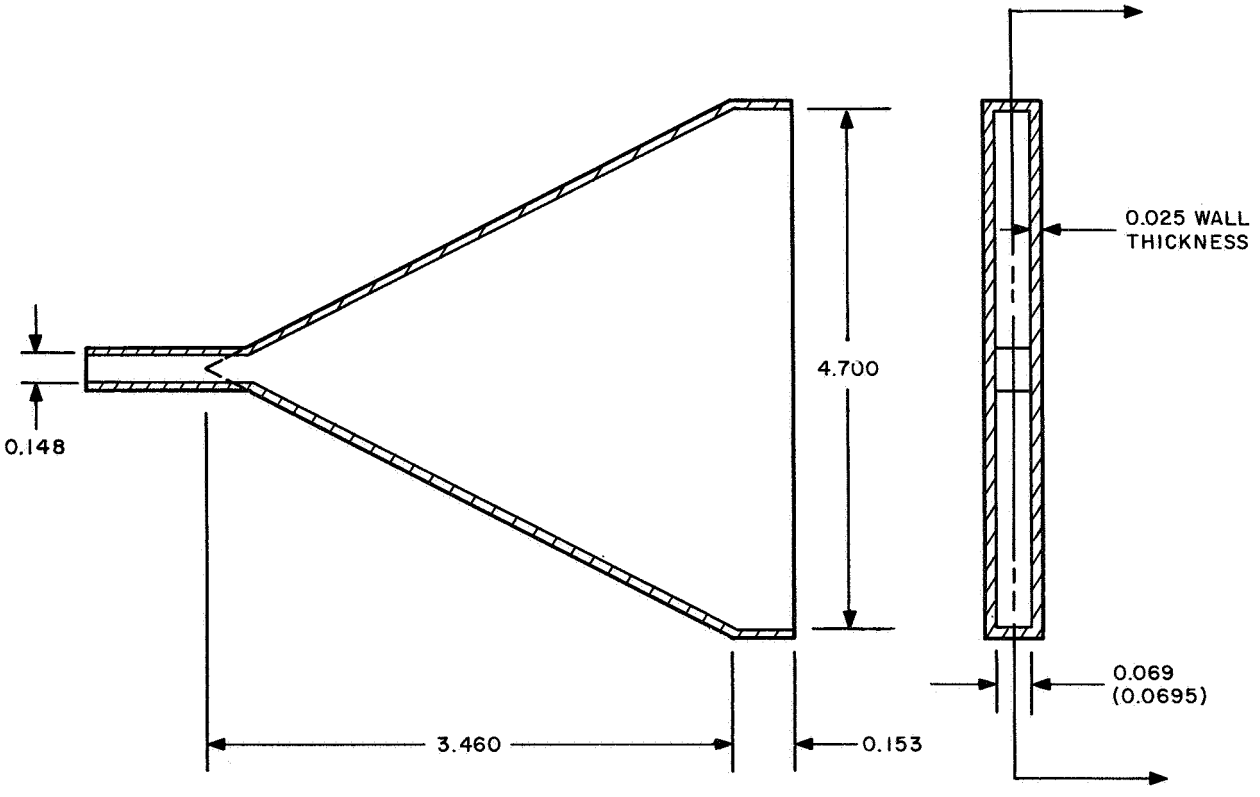

Figure 3. Horn Radiating Element Dimensions

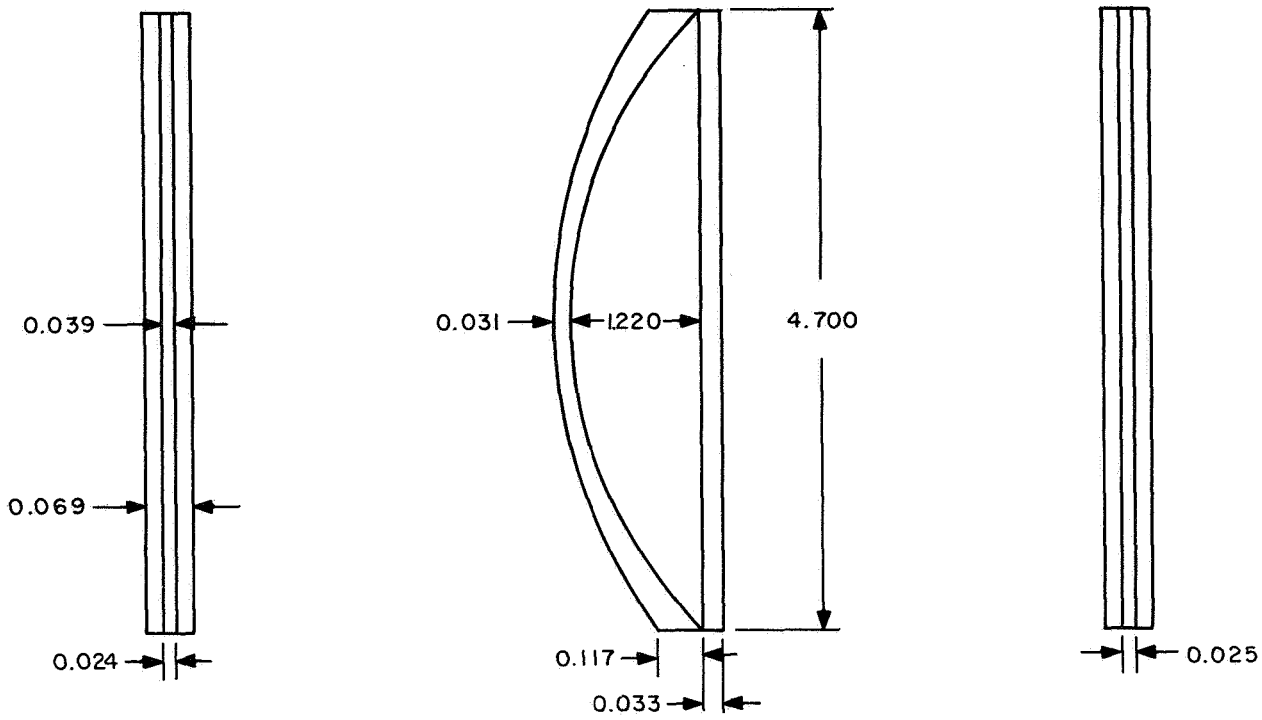

Figure 4. Lens for Radiating Element

surfaces is shown in Figure 5. Morita and Cohn (Ref. 3) give a design procedure for such an impedance matching scheme. The corrugation dimensions calculated using this design procedure are shown in Figure 5 and may be seen to be no more substantial than those of the longitudinal ridge. Thus, the basic design of Figure 4 will be retained for further development effort.

Power Combiner Horn and Mode Generator

A direct scaling of the 16 GHz E-plane power combiner horn and dual LSE_{11} mode generator to 60 GHz yields the configuration illustrated in Figure 6. The dividing wall, shown dotted, was used only for structural purposes in the 16 GHz power combiner and, because it is perpendicular to the electric-field vector in the horn, it can be removed with no ill effect. The input waveguide dimensions were not scaled, but are those of standard waveguide.

Dielectric Lens For Power Combiner Horn

Since the power combiner horn for operation at 60 GHz is essentially a result of direct scaling from the 16 GHz model, the lens design obtained by direct scaling

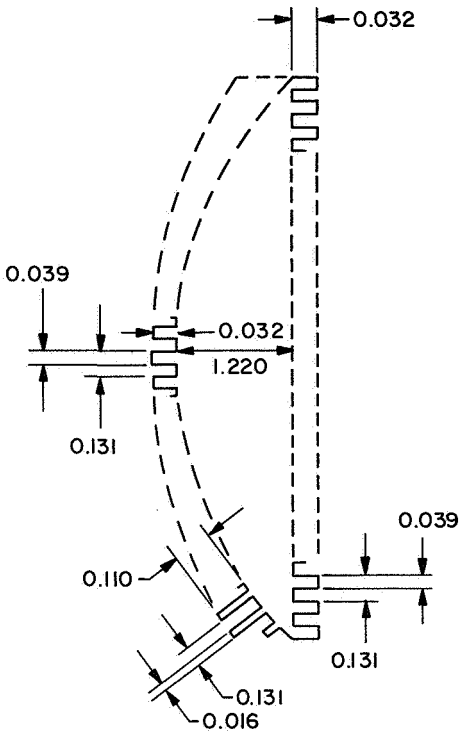

Figure 5. Dimensions of Corrugated Impedance Matching Structure for Radiating Element Lens

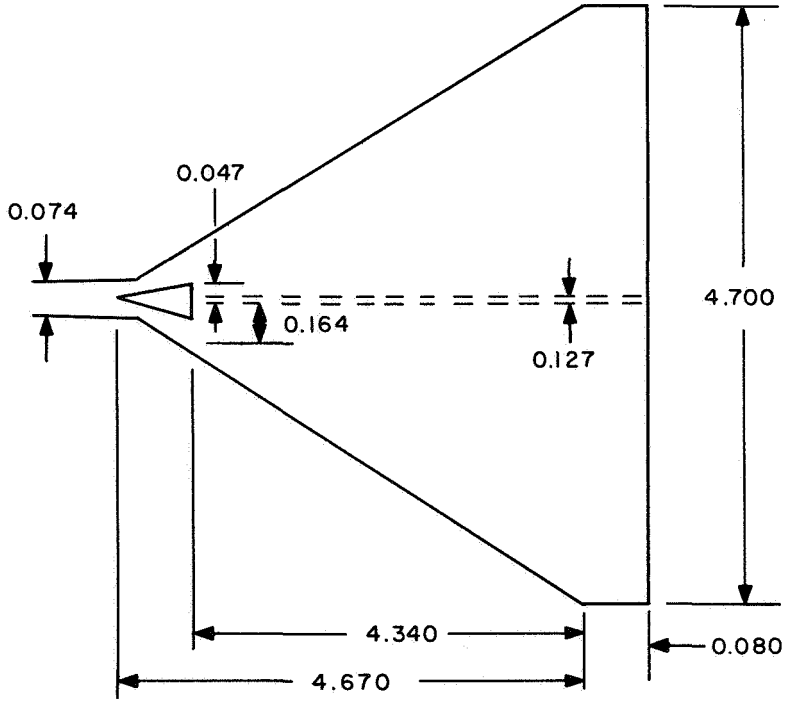

Figure 6. Directly Scaled Power Combiner Horn and Mode Generator

will be retained. The pertinent dimensions of the lens are shown in Figure 7. The portion of the lens formerly occupied by the dividing wall of the horn in shown dotted. It will be shown in the next section that a modification of the power combiner lens allows for the elimination of the septated waveguide and impedance matching section.

Septated Waveguide and Impedance Matching Section

The septated waveguide and impedance matching section (referred to in Ref. 2 as the "divider" section) was used in the 16 GHz array model to provide a transition from the oversize height of the power combiner horn to the stack of fifty waveguides which is the output from the horn array. It was conceived as a separate section rather than an integral part of the horn array merely for ease of fabrication. In essence, the septa in this extra section are a continuation of the broad walls of the output waveguides of the horn array. The thickness of the walls is reduced over one-quarter wavelength to obtain an impedance match to the region which contains no septa. The dimensions resulting from scaling the corresponding section in the 16 GHz model are shown in Figure 8. The transformer sections which step from 0.025 inch to 0.011 inch would cause some manufacturing problems. It would, therefore, be advantageous to eliminate this section completely.

The lens-compensated E-plane power combiner horn may be butted directly against the input waveguides of the array of fifty H-plane horns providing that the impedance matching ridge on the flat side of the power combiner lens is changed. The matching ridge would be used not for an impedance match from dielectric loaded waveguide to empty waveguide, but from dielectric loaded waveguide to a waveguide of the same height divided into fifty parts along its height by walls of finite thickness. This configuration is shown in Figure 9.

The ridge may be designed based on the model shown in Figure 10. Here the output of the lens loaded horn is represented by a waveguide of height b_1 and width a loaded with a dielectric of relative permitivity (ϵ_r) ϵ_1. The matching transformer section is also of height b_1 and width a. The transformer consists of a slab of dielectric (actually an integral part of the lens) centrally located in the guide and extending the entire guide height. The slab has thickness T and length L. The divided section is modeled as a waveguide of height b_2. The dimension b_2 is the difference between b_1 and the sum of the thicknesses of the dividing walls between the H-plane horns. Vartanian, et al (Ref. 4) have assembled extensive data on the propagation constants and impedance of slab loaded waveguide. Using their data, we find the design values of T and L are:

$$T = 0.044 \text{ inch}$$

$$L = 0.041 \text{ inch}$$

Thus, the septated waveguide and matching section can be eliminated.

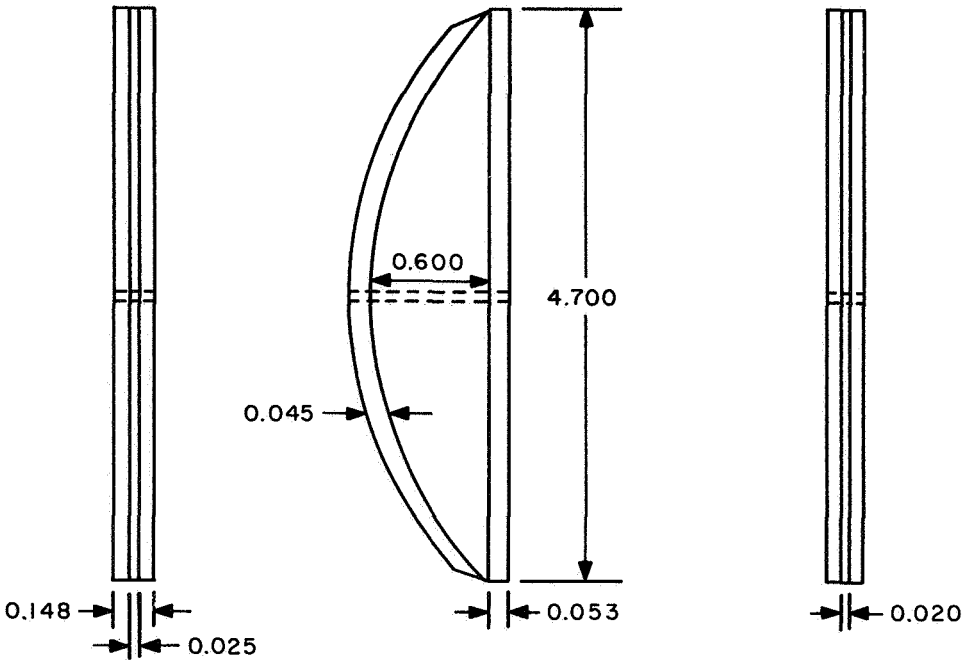

Figure 7. Power Combiner Lens

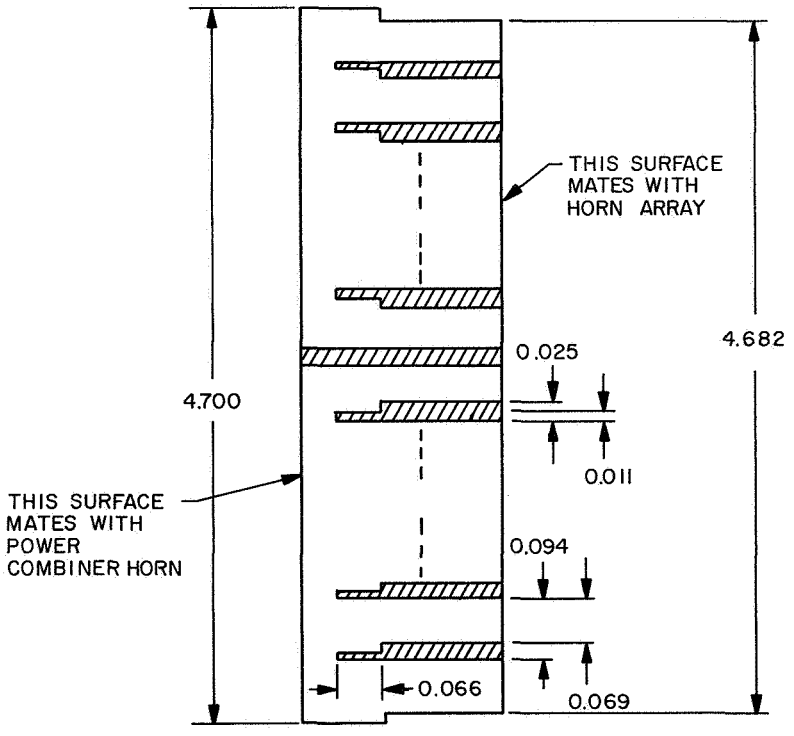

Figure 8. Cross Section of Septated Waveguide and Impedance Matching Section

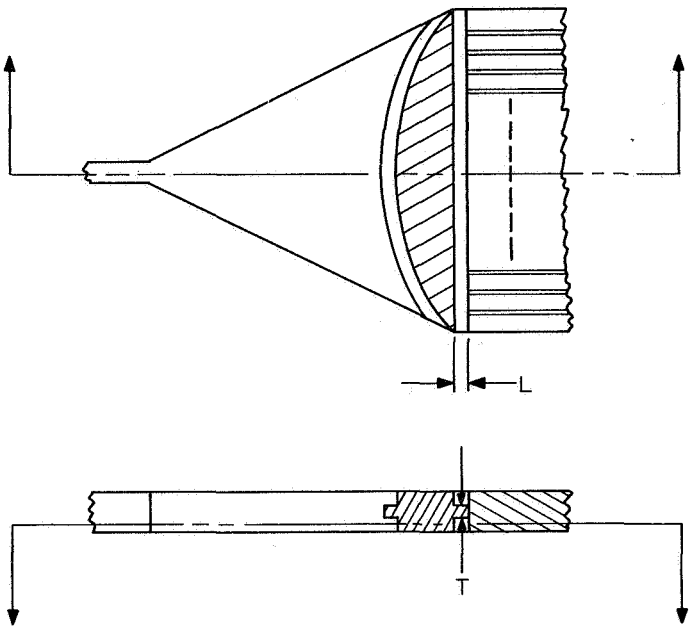

Figure 9. Impedance Matching Section Integrated into Power Combiner Lens

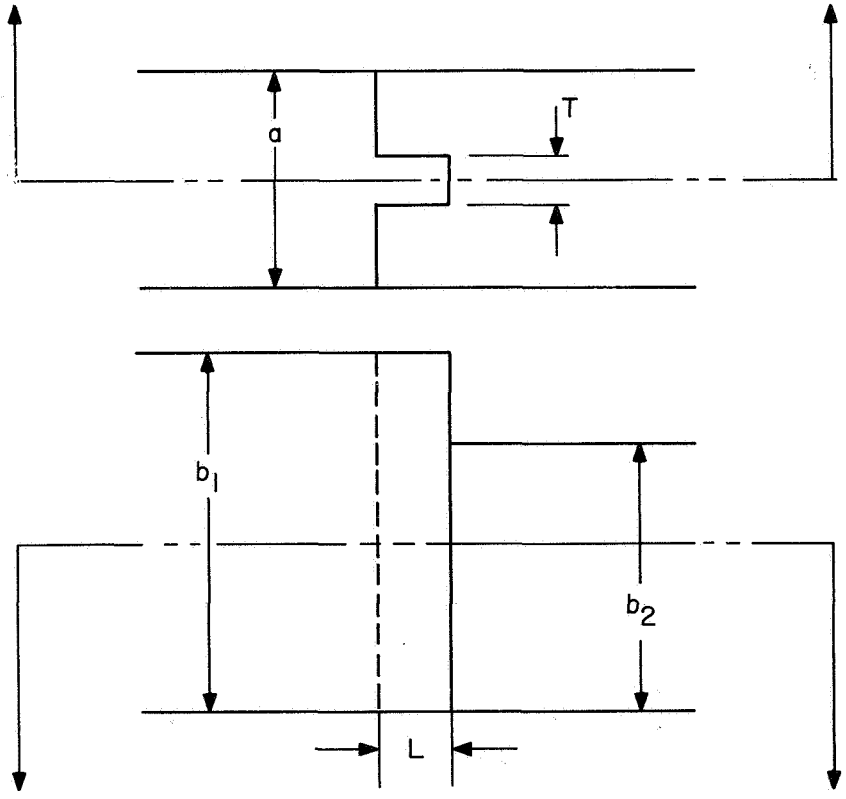

Figure 10. Equivalent Waveguide Model for Modified Impedance Matching Ridge Design

FERRITE PHASE SHIFTER

Beam steering requires that there be some means of providing specific amounts of phase delay in the transmission line between the power combiner and the radiating elements. Several different electronic phase shift methods are currently in use and all but one of these will be eliminated for various reasons. First there is the diode phase shifter. These have been found to be extremely lossy even at X-band and will be discarded immediately.

The next approach is the Reggia-Spencer type of phase shifter. These have been successfully constructed for use at 60 GHz and are, in fact, available as catalog items. The main problem with this approach is that the Reggia-Spencer phase shifter requires a rather large magnetization current to maintain a given phase shift. Thus, almost every phase shifter always requires an excitation current at all times. Also, since the ferrite magnetization is obtained using a solenoid which has considerable self-inductance, switching time of the device is quite slow. The large amount of average power required for these phase shifters and the packaging problem arising from the phase shifter size being a good deal larger than standard waveguide dimensions are sufficient cause to eliminate this phase shifter design.

The last candidate is the latching ferrite phase shifter. This phase shifter can be packaged in a standard size waveguide and only pulse power is required when a change of phase is desired. The latching ferrite phase shifter ostensibly has the most desirable characteristics but very little has been done with these devices at frequencies of the order of 60 GHz.

Very few (Refs. 5, 6) ferrite phase shifters have been built and evaluated at millimeter wavelengths. The results reported on have been characterized by high insertion loss and, hence, a corresponding low figure of merit.

A ferrite phase shifter was constructed at RCA Princeton Laboratories and evaluated to obtain a better understanding of the loss mechanism in the device and to try out a construction approach slightly different from that previously used for lower frequency phase shifters. The material selected was a commercial ferrite, Trans-Tech TT2-111, which is a nickel zinc ferrite with a high saturation magnetization. This material was available in bar stock, and this factor determined the fabrication approach. Two U-shaped pieces with a 0.007 inch wide groove were carefully ground to a final size of 0.074 inches high, and 0.024 inches wide as shown in Figure 11. The transcendental propagation equation which describes a waveguide partially loaded with a material possessing tensor susceptibility was solved numerically with a digital computer. The computer solutions gave estimates for expected phase shift with and without the slot loaded with dielectric. Unfortunately, the experiment was not an unqualified success. Phase shift information was not obtainable because the presence of the gaps in the U-shape reduced the remanent magnetization to an extremely low level. This observation was experimentally verified further when a B-H hoop of the toroid was drawn. Some significant information was provided by the experiment.

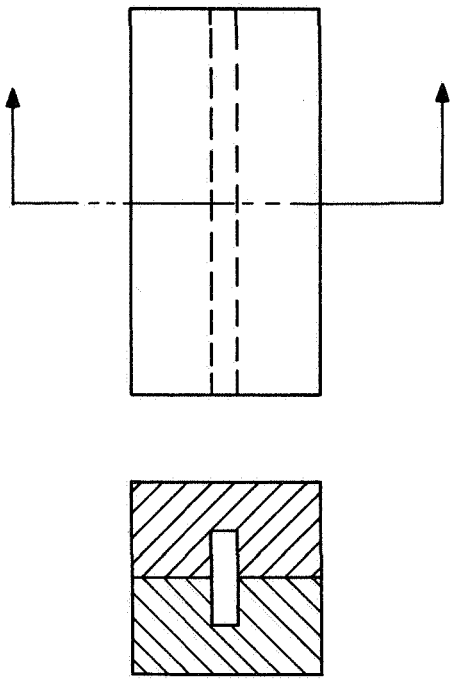

Figure 11. Two Section Ferrite Toroid

A VSWR of 1.2:1 was obtained and the measured insertion loss of the device was less than 1.0 dB per inch. A strong coupling to dielectric loss was observed for some adhesives and slabs used for dielectric loading. Based on this finding for the insertion loss, and the results of the computer program for phase shift, a figure of merit of approximately 250° per dB can be anticipated with this material although this figure is somewhat optimistic. A typical figure of merit for a C-band phase shifter is 514° per dB.

To pursue this anticipated figure of merit experimentally, the following program has been initiated at RCA Princeton Laboratories. A nickel zinc ferrite is being prepared in which the finished slot will be approximately 0.003" wide. Using a toroid which has no gaps, it is anticipated that the phase shift will be close to that obtained using the computer while the insertion loss remains the same as measured before. This figure of merit is very strongly associated with the dielectric loading of the slot. It was observed that the loading material tested, while satisfactory at "X" band frequencies, gave high losses at 60 GHz. If no loading is employed with a 0.007 inch slot, the expected figure of merit reduces to approximately 100°/dB. Thus, for 360° phase shifter with an unloaded 0.007 inch slot, approximately 3.5 dB of loss can be anticipated. It is hoped, therefore, to avoid the need for slot loading by making the slot very small (0.003 inch).

Another factor in the inefficient operation of ferrite material at 60 GHz relates to the very low value of the ratio $\frac{\gamma \times 4\pi M_s}{f_o}$. M_s is the saturization magnetization of the ferrite, f_o is the operating frequency, and γ is a material constant which varies slightly from material to material. This ratio has been a good index to indicate efficient usage of ferrite materials. The ratio also indicates the onset of low-field loss phenomena. Usually the device designer will try to work with a ratio of between 0.5 and 0.8. In this case, with f_o equal to 60 GHz, the ratio is approximately 0.05. Since the maximum value for $4\pi M_s$ of any known ferrite is about 5000 gauss, a fundamental deficiency is revealed. This factor pointed out the need for a new approach.

A different class of materials, referred to as hexagonal ferrites, offers an atractive approach to the problem of material selection at millimeter wavelengths. This new class of hexagonal ferrites may be prepared to have an easy plane and consequently a hard direction of magnetization. The difference in energy levels to pull a magnetization vector out of the easy plane into the hard direction is called the crystalline anisotropy energy. This energy which can be varied by chemical composition adjustment is usually in the range from zero to 100,000 Oersteds. This anisotropy energy appears also in the equations of motion for the magnetic moment. A theoretical analysis (Ref. 7) has been performed and shows that the easy plane configuration would be suitable for the fabrication of a ferrite phase shifter utilizing this anisotropy energy. This analysis indicates that the phase shift provided by the ferrite is again directly proportional to the magnetization but inversely proportional to $\left[\left(\frac{\omega_o}{\omega}\right)^2 - 1\right]$ where ω_o and ω are the resonance and operating angular frequencies respectively. Accordingly, the hexagonal ferrite can be made to exhibit a much higher resonance frequency resulting in a much more desirable efficiency ratio than any conventional ferrite. A hexagonal material will be prepared and fabricated at RCA Princeton Laboratories to test these conclusions. Thus, at this time no conclusive information is available to evaluate a 60 GHz latching ferrite phase shifter.

EXPECTED PERFORMANCE

Several factors must be considered to realistically predict the performance of the array. In this section, errors arising in the antenna will be related to array performance. Array errors may be categorized as systematic errors and random errors.

The principal systematic error is due to the quantization of the phase drive used to electronically steer the antenna beam and will be treated first. The effects of random errors are looked at next. The basic approach of a statistical analysis which closely follows Allen (Ref. 8) is presented. The statistics of the error contributions are computed

and the sidelobe performance is predicted from a purely statistical viewpoint. The effects of random errors due purely to the ferrite phase shifters are then demonstrated by computing representative array patterns including the effects of these errors.

Systematic Errors - Phase Quantization

Specific amounts of phase delay must be incorporated into the excitation of each element to scan the array pattern to a given position in space. The phase delay is generally quantized in order to simplify the computation required to arrive at the necessary phase delays for each element and also to simplify the drive circuitry which provides these delays. In addition, the phase shifters used to obtain these phase delays often are capable of providing phase shift in discrete increments only. The phase shift increments are generally coded in a binary manner so that a given driving phase is obtained from the sum of any of the following possible phase shifts:
$0, \frac{2\pi}{2^n}, \frac{2\pi}{2^{n-1}}, \ldots \pi$ radians. These values are for an n-bit phase shifter. This phase quantization will obviously introduce an error.

The quantization error is illustrated in Figure 12. The desired phase distribution is a straight line but the actual phase is a staircase. The difference between the two is the phase quantization error which is periodic and will give rise to sidelobes. Finer increments of phase, corresponding to larger values of n, result in phase quantization lobes of lower level. Miller (Ref. 9) shows that, if a 5-bit phase shifter is used, the sidelobes due to phase quantization errors remain below 30 dB. The phase increment for this choice is $\frac{\pi}{16}$ radians or 11-1/4 degrees and is the quantization increment which will be chosen for the array under discussion.

Random Errors - Statistical Analysis

Random departures from the ideal amplitude and phase array excitation will result in deteriorated pattern performance. It is the purpose of this section to indicate the sources, statistics, and effects of these random errors. In doing this, the work of Allen (Ref. 8) will be utilized.

The pattern of the ideal array is given formally by

$$F_o(\theta, \phi) = f(\theta, \phi) \sum_{n=0}^{N-1} a_n^{jn(u-u_o)} \tag{1}$$

where

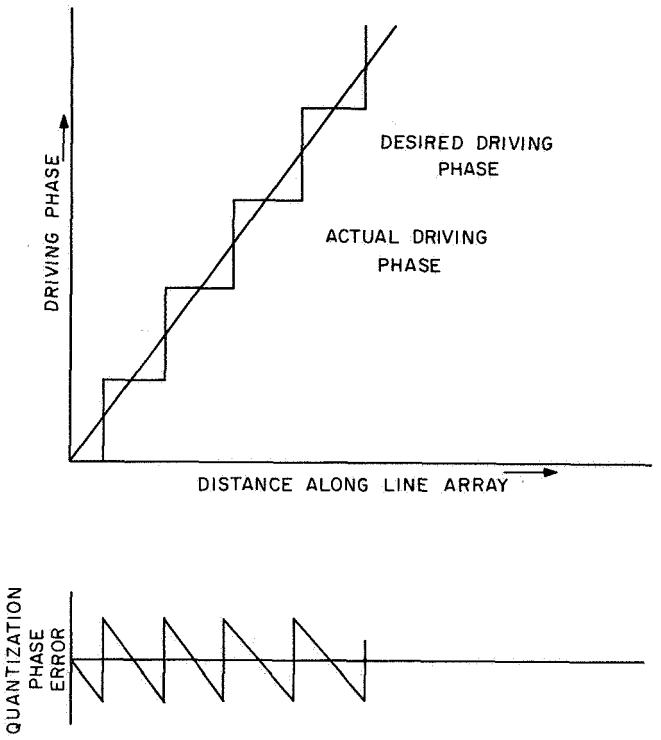

Figure 12. Phase Quantization Error

$f(\theta, \phi)$ is the ideal element pattern function; N is the number of elements in the array; a_n is the amplitude excitation coefficient of the n^{th} element; $u = \frac{2\pi D}{\lambda} \sin \theta$, $u_o = \frac{2\pi D}{\lambda} \sin \theta_o$ where D is the inter-element spacing, θ_o is the angle to which the peak of the beam is scanned, and λ is free space wavelength; and, the coordinate system is shown in Figure 13.

Rather than the pattern given by equation (1) we would obtain the pattern

$$F(\theta, \phi) = \sum_{n=0}^{N-1} f_n(\theta, \phi)\, a_n'\, e^{jn(u-u_o)}\, e^{j\delta_n} \qquad (2)$$

where $f_n(\theta, \phi)$ is the actual element pattern of the n^{th} element; a_n' is the value of a_n with error; and, δ_n is the phase error associated with the n^{th} element.

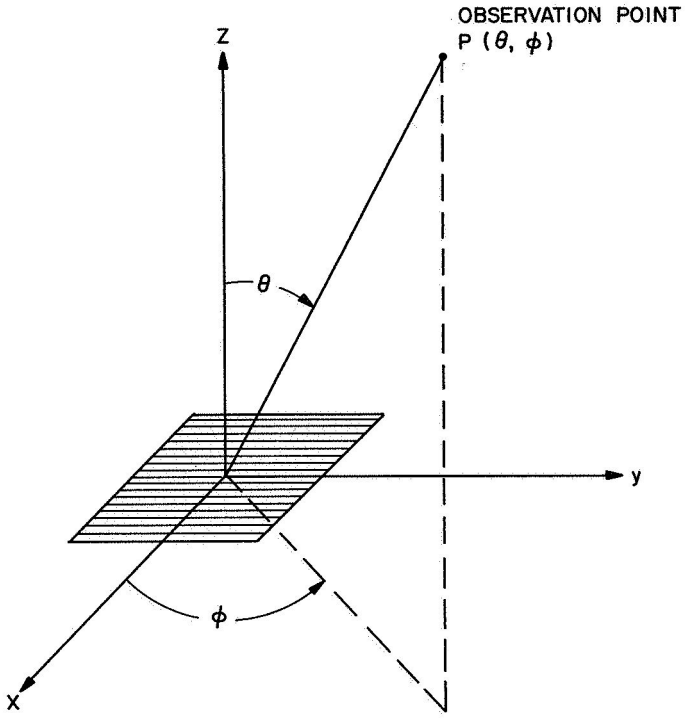

Figure 13. Array Pattern Coordinate Geometry

Amplitude errors arise from several sources. First, if the ideal element pattern function $f(\theta,\phi)$ is thought of as the mean of the actual element pattern functions, $f_n(\theta,\phi)$ may be expressed as

$$f_n(\theta,\phi) = \left[1 + \Delta_n^{(e)}(\theta,\phi)\right] f(\theta,\phi) \tag{3}$$

where the $\Delta_n^{(e)}$ are samples of a random variable with zero mean and variance σ_e^2.

Amplitude errors in the element drive may be attributed to variations in the input E-plane dimensions of the H-plane horn array since it is these dimensions which determine the power delivered to each of the elements. Manufacturing tolerances will also give rise to differences in the insertion loss of different phase shifters. Other factors such as imperfections in the power combiner lens matching surfaces or in the lens itself may give rise to amplitude errors. These, however, should be very small judging from experience at 16 GHz. The coefficient a_n' is, therefore, given by

$$a_n' = \left[\Delta_n^{(p)} + \Delta_n^{(c)} + 1\right] a_n \tag{4}$$

where $\Delta_n^{(p)}$ is the random error due to phase shifter insertion loss and $\Delta_n^{(c)}$ is the random error due to imperfect power split. Both these random variables have zero mean and, $\Delta_n^{(p)}$ and $\Delta_n^{(c)}$ have variances σ_p^2 and σ_c^2 respectively.

Phase errors which enter into consideration for the array configuration of interest are due to lens imperfections, phase shifter tolerances, variations in the cut-off dimension of the 50 waveguide inputs to the H-plane horn array, and errors in the locations of the radiating elements within the array. The phase errors and their variances are tabulated below. All have zero mean.

ERROR	SYMBOL	VARIANCE
Power combiner	$\delta_n^{(c)}$	σ_{pc}^2
Phase shifter insertion phase	$\delta_n^{(I)}$	σ_I^2
Phase shifter bit errors	$\delta_n^{(i)}$	σ_i^2
Waveguide cutoff dimension	$\delta_n^{(w)}$	σ_w^2
Element location	$\delta_n^{(L)}$	σ_L^2

The pattern with errors may be obtained by substituting the error terms into equation (2). This gives

$$F(\theta,\phi) = f(\theta,\phi) \sum \left[(1 + \Delta_n^{(e)}) \; (1 + \Delta_n^{(c)} + \Delta_n^{(p)}) \cdot e^{j(\delta_n^{(c)} + \delta_n^{(i)} + \delta_n^{(I)} + \delta_n^{(w)} + \delta_n^{(L)})} \cdot e^{jn(u - u_o)} \right] \tag{5}$$

Since the probable sidelobe characteristics of the array are of interest, it is the mean square absolute value of equation (5) which is of value. This may be shown to be

$$\overline{F(\theta,\phi)^2} = \left[C^2 \, \delta_n^{(c)} \, (1) \, C^2 \, \delta_n^{(I)} \, (1) \, C^2 \, \delta_n^{(i)} \, (1) \, C^2 \, \delta_n^{(w)} \, (1) \, C^2 \, \delta_n^{(L)} \, (1) \right]$$

$$\cdot f^2(\theta,\phi)\left|\sum a_n e^{jn(u-u_o)}\right|^2$$

$$+ f^2(\theta,\phi)\left\{\left[1+\sigma_e^2+\sigma_c^2+\sigma_p^2\right]\right.$$

$$\left.- C^2\,\delta_n^{(c)}(1)\,C^2\,\delta_n^{(I)}(1)\,C^2\,\delta_n^{(i)}(1)\,C^2\,\delta_n^{(w)}(1)\,C^2\,\delta_n^{(L)}(1)\right\}$$

$$\cdot\left|\sum a_n^2\right|$$

where

$$C_\tau(\alpha) \overset{\Delta}{=} \int_{-\infty}^{\infty} e^{j\alpha\tau}\,p(\tau)\,d\tau$$

is the characteristic function for the random variable τ.

If $\sigma_\tau^2 << 1$ then the characteristic function may be approximated by

$$C_\tau(\alpha) \approx 1 - \frac{\alpha^2\sigma_\tau^2}{2}$$

and

$$C_\tau^2(\alpha) \approx 1 - \alpha^2\sigma_\tau^2 \tag{6}$$

Using this in equation (5) gives

$$\overline{\left|F(\theta,\phi)\right|^2} = f^2(\theta,\phi)\left[(1-\sigma_{phs}^2)\left|\Sigma a_n e^{jn(u-u_o)}\right|^2 + (\sigma_{amp}^2+\sigma_{phs}^2)\left|\Sigma a_n^2\right|\right] \tag{7}$$

where

$$\sigma_{phs}^2 = \sigma_{pc}^2 + \sigma_I^2 + \sigma_B^2 + \sigma_w^2 + \sigma_L^2 \qquad \text{(a)}$$

and (8)

$$\sigma_{amp}^2 = \sigma_e^2 + \sigma_c^2 + \sigma_p^2 \qquad \text{(b)}$$

The sidelobe-ratio variance is given by

$$\sigma_R^2 = \frac{\overline{|F(\theta, \phi)|^2} - \overline{|F(\theta, \phi)|}^2}{\overline{|F(\theta_o, \phi_o)|}^2}$$

Using equations (2) and (5) it can be shown that

$$\sigma_R^2 = \frac{f^2(\theta, \phi)}{f^2(0, 0)} \frac{\sigma_{amp}^2 + \sigma_{phs}^2}{2(1-\sigma_{phs}^2)\eta_a N} \tag{9}$$

where (θ_o, ϕ_o) is the position of the peak of the beam; $(0, 0)$ is broadside; and, η_a is the aperture efficiency which may be calculated from

$$\eta_a = \frac{\left|\Sigma a_n\right|^2}{\Sigma \left|a_n\right|^2} \tag{10}$$

It must be emphasized that both equations (7) and (9) are only valid for $\sigma_{amp}^2 << 1$ and $\sigma_{phs}^2 << 1$.

Since sidelobe performance is of primary concern, the ratio of electric field intensity at a point in the sidelobe region to the field intensity at the peak of the beam is of use. This is given by

$$R(\theta, \phi) = \frac{|F(\theta, \phi)|}{|F(\theta_o, \phi_o)|}$$

Letting $R_m(\theta, \phi)$ be the no-error sidelobe level at the specific location (θ, ϕ), the probability that the actual sidelobe level is less than some threshold R_T is given by the expression

$$P\left[R(\theta, \phi) \le R_T \,\middle|\, R_m\right] = \int_0^{R_T} \frac{R}{\sigma_R^2} I_o\left(\frac{R R_m}{\sigma_R^2}\right) \exp\left[-\frac{R^2 + R_m^2}{2\sigma_R^2}\right] dR \tag{11}$$

where I_o is the modified Bessel function of the first kind of zero order. Equation (11) was the ultimate object of this analysis and its evaluation will give some insight into the sidelobe performance of the array.

The necessary tools for evaluating the effects of errors have been presented and it is now necessary to specify the statistics of the various errors. Considering the amplitude errors first, the variance of the element factor error is approximately

0.005 in the sidelobe region of the array pattern. This value was obtained by considering the measured element patterns of the 16 GHz 10-element array model. Although 10 points hardly comprise a huge sample space, it should be sufficiently large to indicate expected variations. The above value of variance is considered pessimistic since the elements are not in their actual array environment and, hence, are subject to greater effects from edge conditions.

The origin of amplitude errors in the power combiner is a direct consequence of the basic principles of operation of the device. The power coupled from any of the 50 adjacent ports is proportional to the cross-sectional area of that port at its junction with the lens compensated horn. Therefore, any errors in that cross-sectional area will result in a corresponding error in the power coupled from that port. It is expected that the waveguide components for the array can be constructed to the standard 60 GHz waveguide tolerance of ±0.001 inch. The anticipated error in cross-sectional area and hence in power will be

$$\Delta_c = \pm \frac{a+b}{ab} \times 0.001 \tag{12}$$

where a and b are the design values of the waveguide width and height respectively. If we assume the errors to be normally distributed and that in 99.99% of the cases Δ_c does not exceed the value given by equation (12), the 3σ value for the amplitude error is given by

$$3\sigma_c = \sqrt{\Delta_c}$$

or

$$\sigma_c^2 = \frac{\Delta_c}{9}$$

The amplitude error due to non-uniformity in the insertion loss of the phase shifters may be estimated from previous experience with ferrite phase shifters designed to operate at C-band. Taking into account the mechanical problems associated with the construction of a 60 GHz ferrite phase shifter, the 3σ value for insertion loss should be about ±0.3 dB. The corresponding variance would be

$$\sigma_p^2 = 1.34 \times 10^{-3}$$

The amplitude error variance given by (8b) is therefore

$$\sigma_{amp}^2 = 6.54 \times 10^{-3}$$

The contributions to the phase error variance must now be considered. Based on measurements made at 16 GHz, the variance of phase error at the output of the power combiner, σ_{p_c} is about 0.002.

The statistics of the ferrite phase shifters will be inferred from data obtained from a large number of phase shifters designed to operate at C-band. It is believed that with sufficient care in construction, the 60 GHz phase shifters may be made to operate within the same phase tolerances. The standard deviation of the phase shifters as obtained from the above experimental program is shown in Table I. Since mechanical tolerances at 60 GHz are so critical, it might be expected that the phase shifter performance would be somewhat worse than observed at C-band. Table I, therefore, also contains what is expected to be the maximum values of standard deviation. The sidelobe performance will be predicted for both cases.

If it is assumed that each of the 32 possible phase shifter settings is equally likely, the variance of errors due to bit setting is given by

$$\sigma_B^2 = \frac{1}{32} \sum_{i=1}^{32} \sigma_i^2$$

since the phase errors of the individual bits are independent. σ_i^2 is the variance corresponding to the i^{th} possible phase shifter setting. For example, if this setting is 135 degrees then

$$\sigma_i^2 = \sigma_{b_2}^2 + \sigma_{b_3}^2$$

TABLE I. STANDARD DEVIATION OF PHASE SHIFTER ERRORS

Error Contribution		Standard Deviation	
		Measured at C-band	Maximum Expected
Insertion Phase	σ_I	±5°	±10°
Bit Setting -			
180° bit	σ_{b1}	±5/3°	±3°
90° bit	σ_{b2}	±5/3°	±3°
45° bit	σ_{b3}	±1°	±2°
22.5°	σ_{b4}	±1°	±2°
11.25°	σ_{b5}	±1°	±2°
Composite Bit Setting	σ_B	±1.464°	±2.74°

Evaluating the expression for σ_B^2 it may be seen that

$$\sigma_B^2 = \frac{1}{2} \sum_{j=1}^{5} \sigma_{b_j}^2 \tag{13}$$

The value of σ_B is shown in Table I.

Waveguide tolerances give rise to phase errors since differences in waveguide cut-off dimensions result in changes of propagation factor. The waveguide tolerance of ±0.001 inch will bring about a maximum phase error between waveguides of ±0.129 radians/inch. Assuming a normal distribution of errors for which this error is the 3σ value and a maximum waveguide length of one inch, the corresponding phase rror variance is

$$\sigma_w^2 = 1.85 \times 10^{-3}$$

The waveguide length of one inch should take care of any connecting waveguide between the power combiner and phase shifters, between the phase shifters and the throats of the H-plane horn radiating elements, and the relatively narrow region of the H-plane horns in the vicinity of the horn throats.

The last source of phase error to be considered is that due to errors in the location of the elements in the array. Since the horn array will most likely be made as a unit, the only element location errors of any significance should be along the X-axis in Figure 13. Although the radiating ends of the H-plane horns have a rather large aspect ratio, the phase compensating lenses act as mechanical spacers. Therefore, phase error due to element errors should be negligible.

Using equation (8a) and the values of the individual phase error variances which have been estimated above, the two values of total phase error variance which will be investigated are

$$\sigma_{phs_1}^2 = 1.21 \times 10^{-2}$$

and

$$\sigma_{phs_2}^2 = 3.65 \times 10^{-2}$$

Now only the aperture efficiency and the ratio

$$R_f = \frac{f^2(\theta, \phi)}{f^2(o, o)}$$

for the angles of interest must be determined to find the sidelobe ratio variance. The aperture efficiency of the array as given by equation (10) is 0.85. The ratio R_f is approximately 0.6 in the region

$$20° \leq \theta \leq 60° \text{ and } 120° \leq \theta \leq 150°$$

Thus the two values of sidelobe ratio variance which are of interest are

$$\sigma^2_{R_1} = 1.34 \times 10^{-4}$$

and

$$\sigma^2_{R_2} = 3.16 \times 10^{-4}$$

The above values of σ^2_R may be substituted into (11) to find the probability that a given sidelobe level will remain below a specified threshold value. The integral was evaluated using numerical techniques and the results are shown in Figures 14 through 16. The three sets of curves correspond, respectively, to the following cases: phase shifter errors neglected; all errors included with phase shifter errors being given by the statistics obtained from measurements at C-band; all errors included with worst anticipated phase shifter errors. Recall that R_m is the pattern level with no errors, R is the pattern level with errors and R_T is the threshold level. Interpretation of the curves is clear from the following example.

Referring to Figure 14 for a no-error sidelobe level of $R_m = -40$ dB the probability that the sidelobe level with errors will be no greater than $R_T = -30$ dB is seen to be $0.997 = P\left[R \leq -30 \text{ dB} \mid R_m = -40 \text{ dB}\right]$. Similarly, the probability that a no-error level of 50 dB is less than 40 dB when errors are taken into account is 0.57. These numbers correspond to the absence of phase shifter errors and thus give an indication of the best possible sidelobe performance.

Looking now at the more realistic case where phase shifter errors are included, it is immediately obvious from a comparison of Figures 14 and 15 that the sidelobe performance will deteriorate. The probabilities corresponding to the same to sidelobe values are now

$$P\left[R \leq -30 \text{ dB} \mid R_m = -40 \text{ dB}\right] = 0.95$$

$$P\left[R \leq -40 \text{ dB} \mid R_m = -50 \text{ dB}\right] = 0.31$$

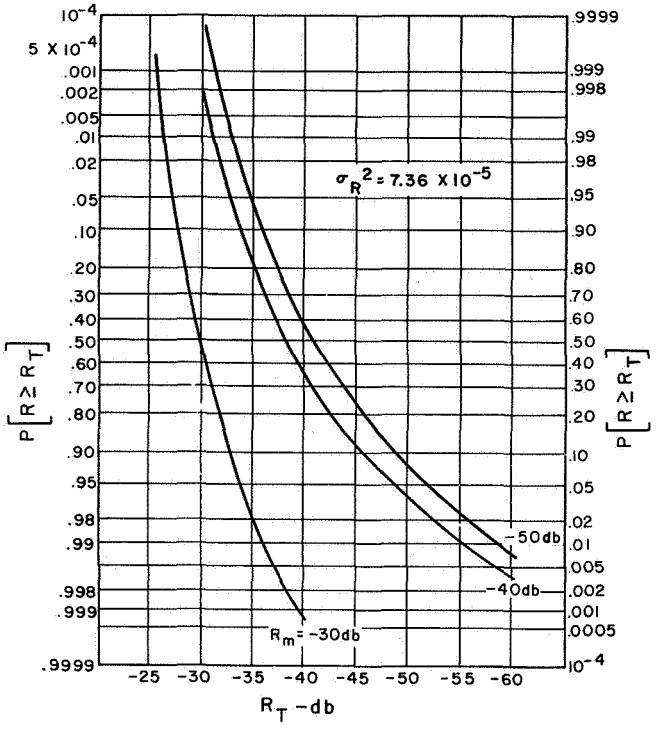

Figure 14. Sidelobe Level Probability, Phase Shifter Errors Neglected

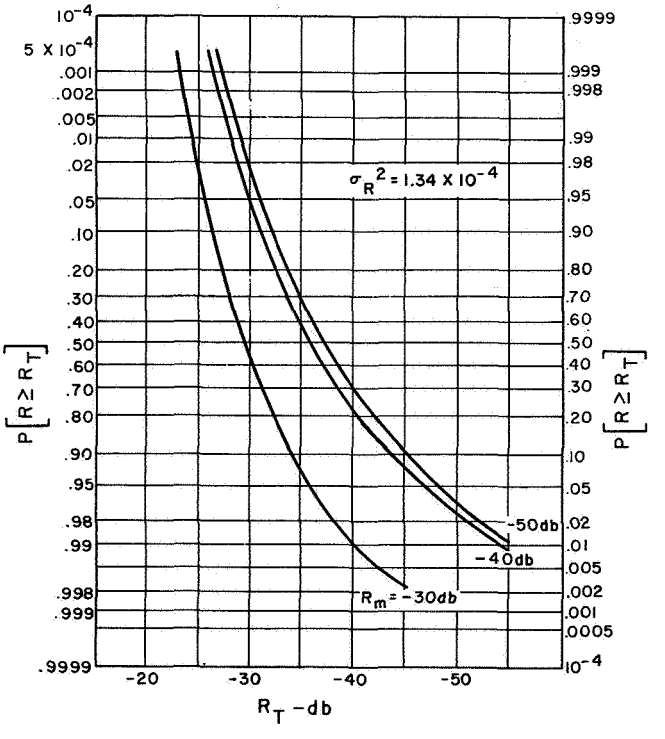

Figure 15. Sidelobe Level Probability, All Errors Included

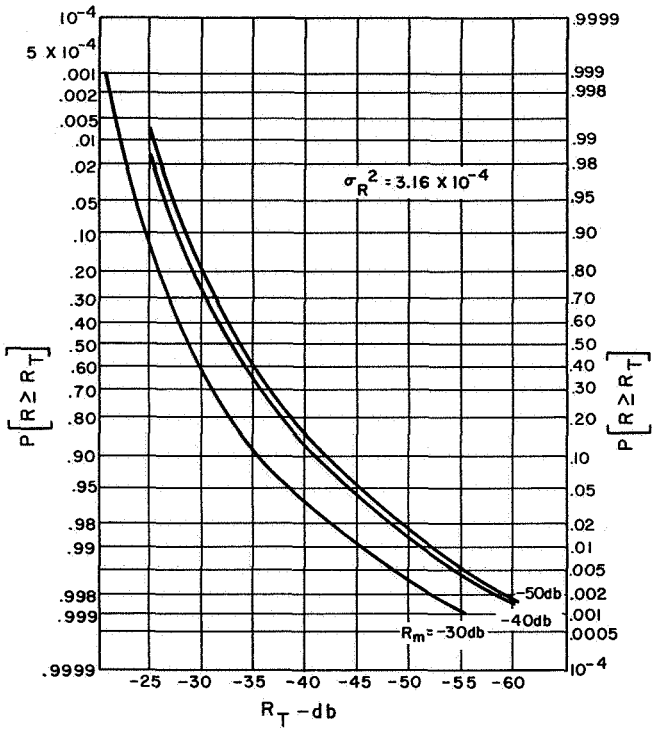

Figure 16. Sidelobe Level Probability, All Errors Included, with Worst Anticipated Phase Shifter Errors

Since most of the no-error sidelobes are less than -40 dB, the sidelobe levels with errors should be below -30 dB with a probability of 0.95 and below -36 dB with a probability of 0.50. Integration of computed patterns in the next section will show that sidelobe levels of -35 dB yields a beam efficiency of the order of 0.90 which is acceptable for the radiometric application of this array although a higher beam efficiency is always desirable.

Quickly inspecting Figure 16 shows that when the worst possible phase shifter errors are considered, a no-error sidelobe level between -40 and -50 dB will result in a sidelobe level expected to be below -27 dB with probability 0.95 and below -33 dB with probability 0.5. This 3 dB deterioration in sidelobe level results in a beam efficiency of the order of 0.8 which is unacceptably low.

Thus, for an array of only 50 elements, the phase shifter errors must not be any worse than those obtained at C-band. Greater phase shifter errors will result in beam efficiencies which are unacceptably low. This conclusion will be supported further by the results of the next section.

Pattern Deterioration Due to Phase Shifter Errors

Since the phase shifters account for the greatest portion of phase error, it would be useful to consider the effects of only the phase shifter errors on pattern performance. The statistical approach of the last section is useful for estimating the expected overall sidelobe performance of the array. The object of this section is to calculate some array patterns including the effect of phase shifter phase errors only. Patterns will be computed for several phase error statistics for a number of scan conditions. The result will be several typical patterns which will illustrate the dependence of sidelobe levels on phase error statistics. This will indicate limits for acceptable phase shifter performance and at the same time give a more vivid picture of sidelobe performance than is available from the purely statistical analysis.

The pattern computation will follow the methods outlined in Profera (Ref. 1). The radiation pattern for the array geometry shown in Figure 13 is given by the following expression:

$$F(\theta, \phi) = f(\theta, \phi) \sum e^{j(\gamma_n + \psi_n)} \left(1 + 0.8 \cos \frac{\pi n}{N}\right) \tag{14}$$

where $f(\theta, \phi)$ is the theoretical element pattern given by

$$f(\theta, \phi) = \frac{1 + \cos \theta}{2} \left(\frac{\sin u \cos v}{u \left[\left(\frac{\pi}{2}\right)^2 - v^2 \right]} \right) \tag{15}$$

and

$$u = \frac{\pi a}{\lambda} \sin \theta \cos \phi$$

$$v = \frac{\pi b}{\lambda} \sin \theta \sin \phi$$

$$\psi_n = -\frac{2\pi}{\lambda} nD \sin \theta \cos \phi \tag{16}$$

$$\gamma_n = \frac{2\pi}{\lambda} nD \sin \theta_o + \delta_{n_p} \tag{17}$$

θ_o is the desired direction of scan, δn_p is the phase error associated with the n^{th} element, and D is the inter-element spacing.

Selection of the δ_{n_p} is based on the assumption that each δ_{n_p} is a sample of a normally distributed random variable with variance σ_δ^2. The δ_{n_p} are obtained using a computer program which generates such a random variable.

As shown in the previous section

$$\sigma_\delta^2 = \sigma_I^2 + \sigma_B^2 \tag{18}$$

where σ_I^2, is the variance of the insertion phase error and σ_B^2 is given by equation (13).

The values of δ_{n_p} are then substituted into equations (14) to (17) to obtain the array patterns.

The two values of phase shifter phase error variance obtained in the last section are used here. The chosen scan conditions are broadside, 20°, 40°, and 60°. The resulting beam efficiencies and patterns are shown in Table II and Figures (17) to (20) respectively. The no-random-error beam efficiencies were included for reference.

TABLE II. BEAM EFFICIENCY

Beam Scanned to	Beam Efficiency		
	$\sigma_\delta = 0$	$\sigma_\delta = 0.091$	$\sigma_\delta = 0.181$
Broadside	0.988	0.956	0.853
20°	0.961	0.903	0.861
40°	0.962	0.904	0.764
60°	0.966	0.933	0.726

The patterns rather vividly show the effects of phase quantization error as well as random phase errors. As predicted, the sidelobes due to phase quantization error as shown in part a of Figures (17-20) ($\sigma_\delta = 0$) remain essentially below -30 dB. The effect of the random errors on the sidelobe structure is clearly illustrated in parts b and c of Figures (17-20).

Inspection of Table II shows that phase shifter errors greater than those obtained at RCA with C-band phase shifters ($\sigma_\delta = 0.091$) are not acceptable if a beam efficiency of the order of 0.90 is desired. Thus the 60 GHz phase shifter performance must be at least as uniform as those previously produced for operation at C-band.

The rather surprising result for $\sigma_\delta = 0.091$ and 60° seen is due to the particular random phase error distribution used for that particular pattern computation. Such improved efficiency with large scan was merely the result of chance and should not be taken to be typical.

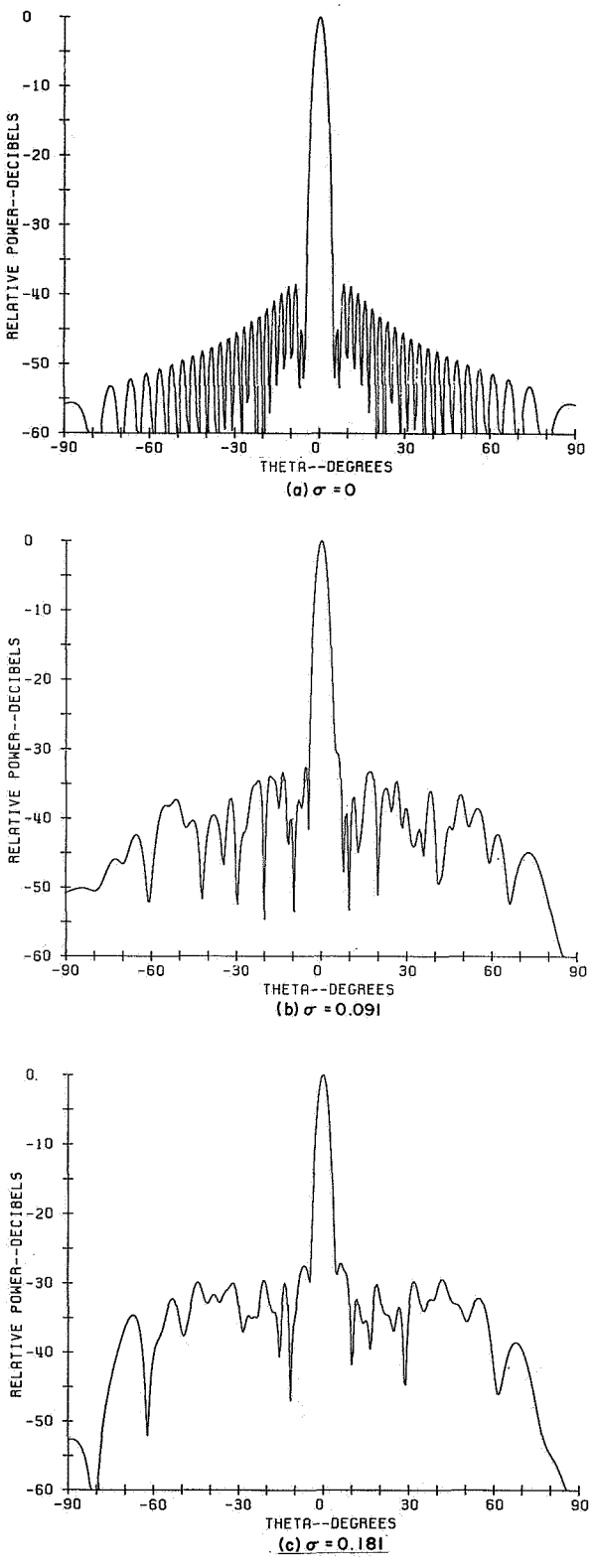

Figure 17. Computed Array E-Plane Pattern Broadside Scan

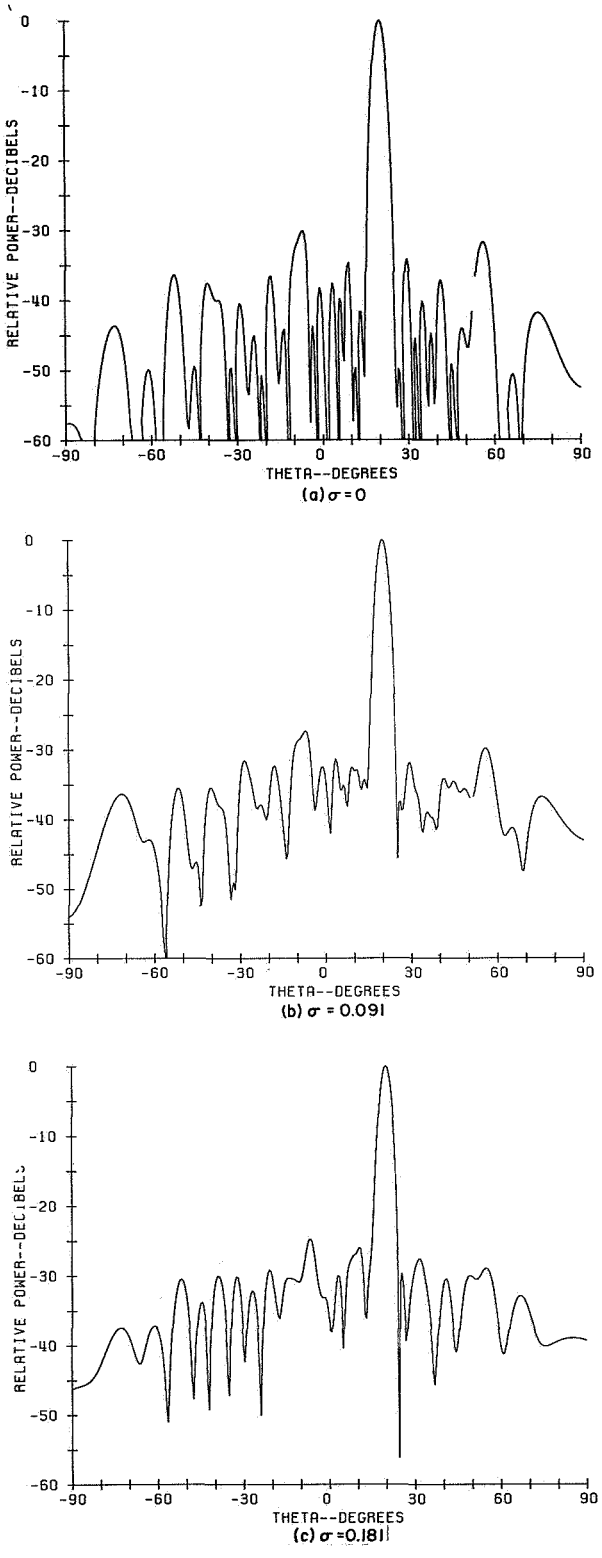

Figure 18. Computed Array E-Plane Pattern Beam Scanned 20° from Broadside

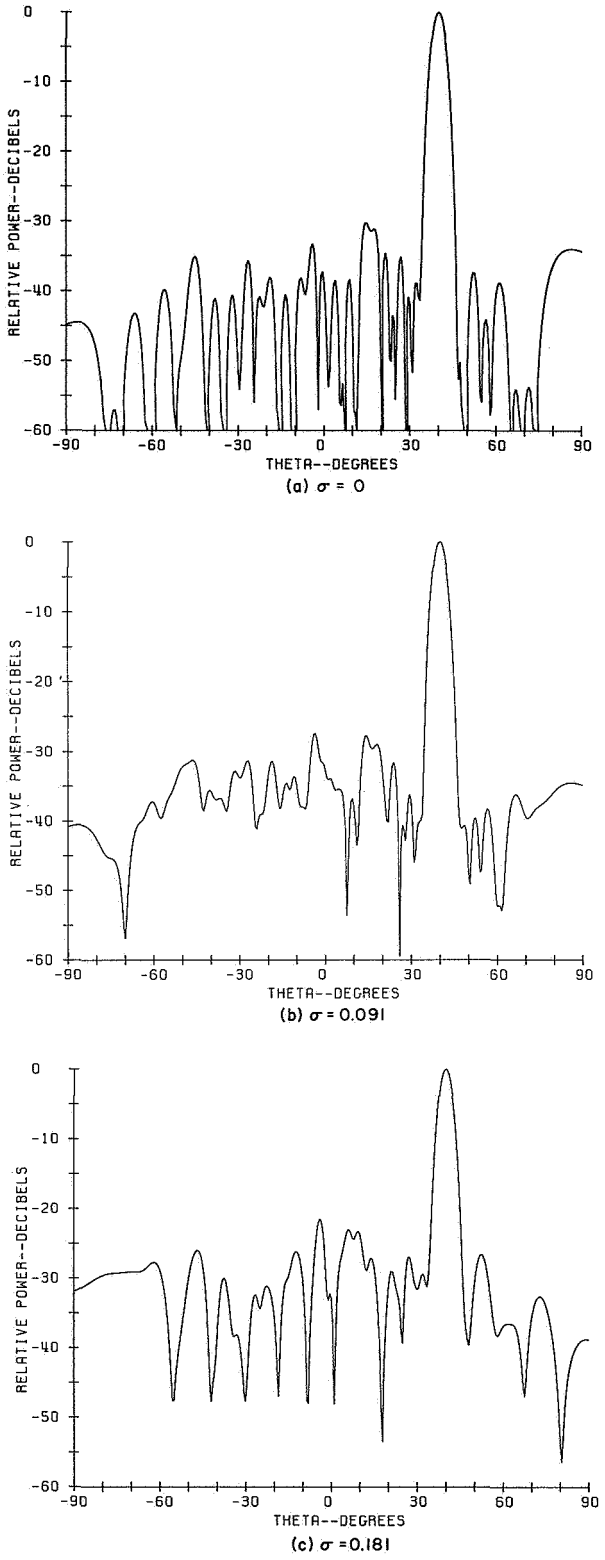

Figure 19. Computed Array E-Plane Pattern Beam Scanned 40° from Broadside

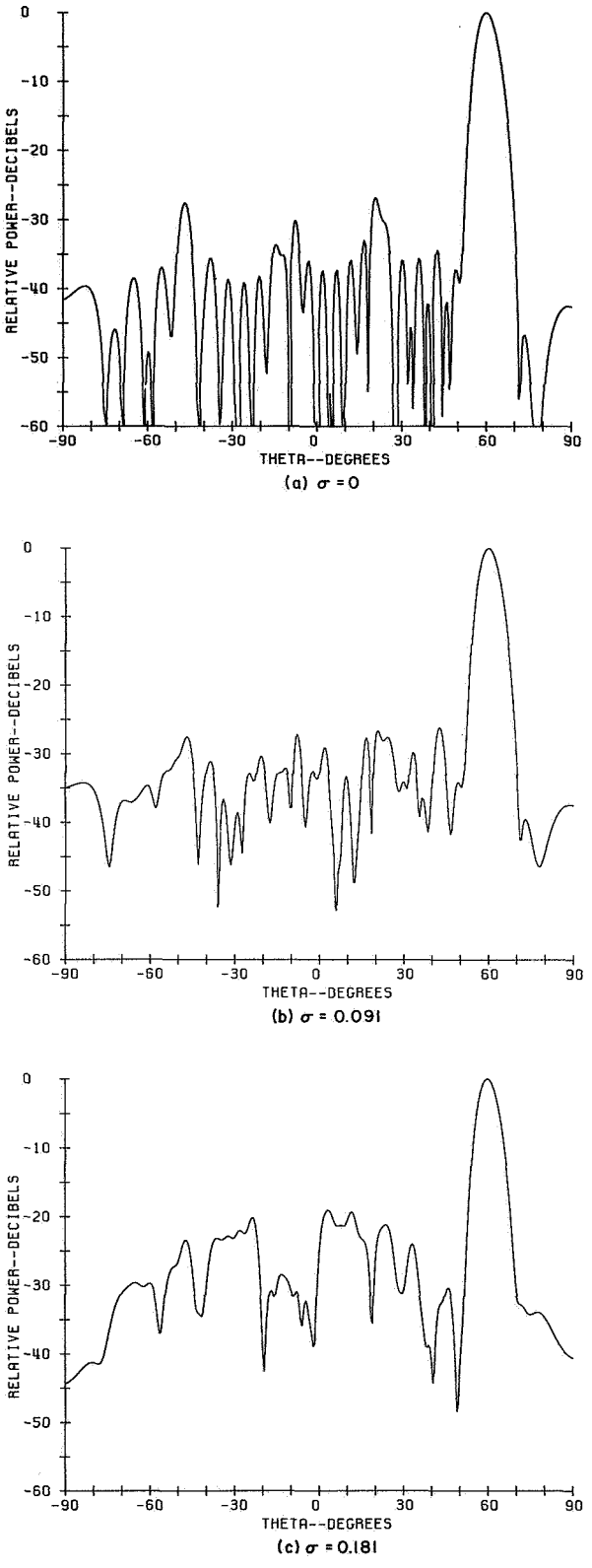

Figure 20. Computed Array E-Plane Pattern Beam Scanned 60° from Broadside

FABRICATION TECHNIQUES

Several fabrication techniques for constructing the 60 GHz array have been considered and explored. These techniques, and their advantages and disadvantages, will be described in this section. Specific recommendations, however, will not be made since most of the techniques require further experimental evaluation. Experimental results which have been obtained will be presented to acquaint the reader with the problems involved and with the extremely small dimensions which often cause the problems.

Horn Array

Two basic methods of constructing the horn array will be given attention. The first of these is the lamination method used at 16 GHz. The second is really a class of methods all of which use electroforming techniques.

Lamination. - The simple lamination technique is straightforward and merely consists of alternating layers of broad walls and side walls as shown in Figure 21. It requires the least new technology and the parts may be produced by conventional machining methods. This method, however, requires a large number of precision machined parts, with the attendent problem of maintaining precision without incurring prohibitive costs. The resulting array contains a large amount of metal necessary only for structural purposes. The array weight would therefore be a good deal greater than if the horn side wall thickness were comparable to those of standard waveguide.

Electroforming. - The basic idea of the electroforming method is to cut the broad walls of the horn from sheet stock, temporarily assemble them with removable spacers, electroplate the side walls on the spacers, and then remove the spacers. The electroforming approach was referred to as a class of methods since there are several different schemes for obtaining the correct spacing between the broad walls, for making the temporary assembly, and for removing the spacers.

One electroforming method consists of embedding the entire horn array in a plastic material. First the horn dividing walls are machined from sheet stock as was done with the lamination method. Now, however, these walls are supported in a fixture which holds the walls at the proper spacing and also temporarily forms the side walls of the array. A possible configuration is shown in Figure 22. The entire array is then filled with a removable molding material and the support fixture is removed leaving what is sketched in Figure 23 a. The side walls are then electroplated on the surface of the molding material after the surface has been coated with a silver solution to make it electrically conductive. This stage is illustrated in Figure 23 b. The side walls are built up on the outside with epoxy or a similar material for added structural strength and the plastic material is then removed with solvents or gentle

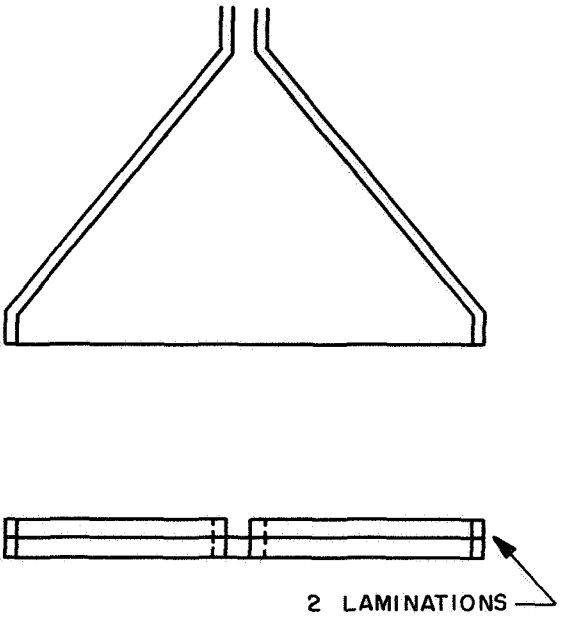

Figure 21. Lamination Method of Construction

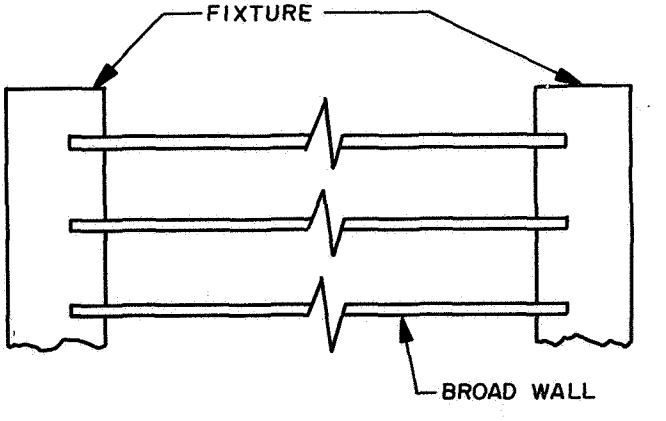

Figure 22. Assembly Fixture for Electroforming Construction Method

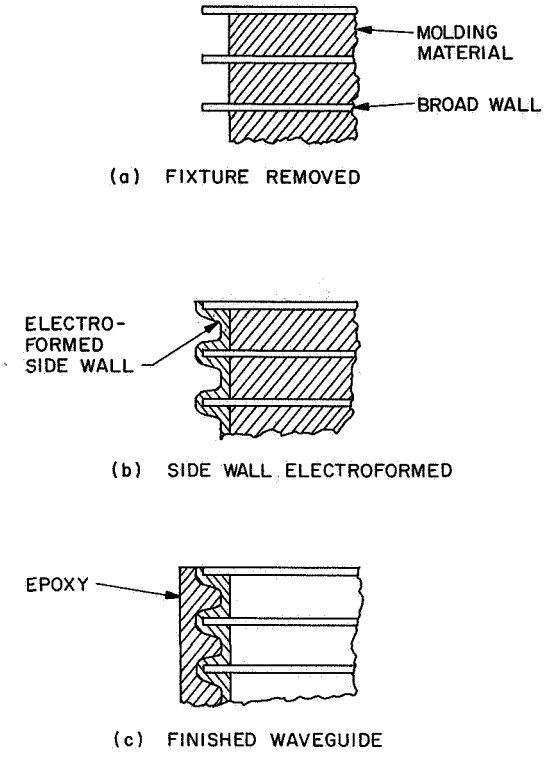

Figure 23. Stages of Electroforming Procedure

heat. Figure 23 c shows this final stage. The weight added by the epoxy material is small compared to a similar amount of metal.

This method was explored experimentally to pinpoint the possible problem areas. The resulting hardware is shown in Figures 24 and 25. The sample in the foreground in Figure 24 and on the bottom in Figure 25 was completely processed. The molding material of the other sample was not removed. This experiment was intended only to evaluate sidewall forming and plating techniques and no effort was made to maintain the broad walls parallel to each other. The molding material was "Rigidax", a stiff wax-type substance which is used primarily for temporarily encapsulating thin walled objects so they can be easily machined. It must be heated beyond its melting point, which is about 150°F, for the molding procedure and it must be remelted to be removed.

The detail shown in Figure 26 points out some of the problems encountered in using this particular construction procedure. Point number 1 shows the result of there being a crevice between the broad wall plate and the slot in the holding fixture. It is quite obvious that some of the molding material flowed into that crevice and the sidewall had not plated to the broad wall. The raggedness of the inner surface of the side walls shown by point 2 occurred because the molding material adhered to the support fixture. When the fixture was removed, some of the molding material remained with it. The copper side wall then plated on the uneven surface that remained.

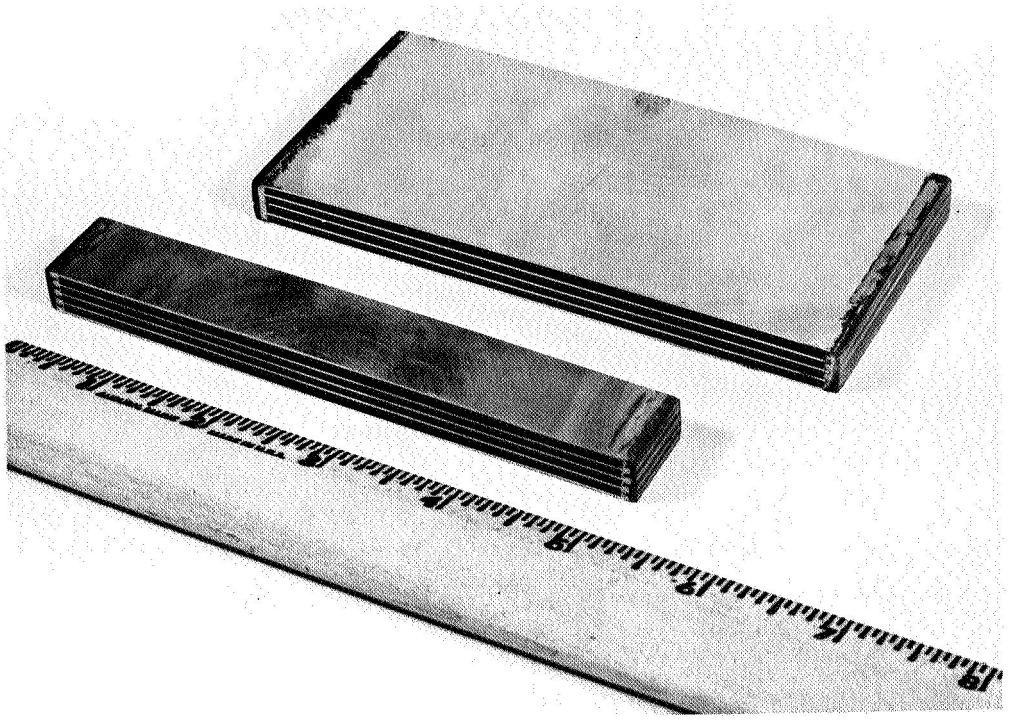

Figure 24. Electroformed Waveguides

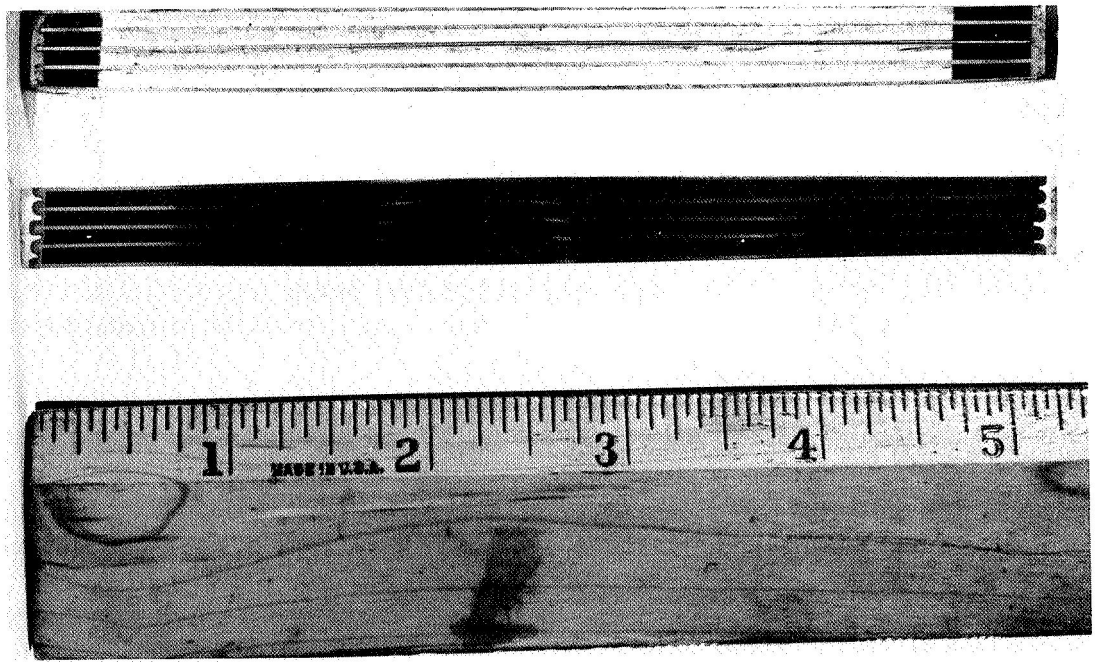

Figure 25. Electroformed Waveguides

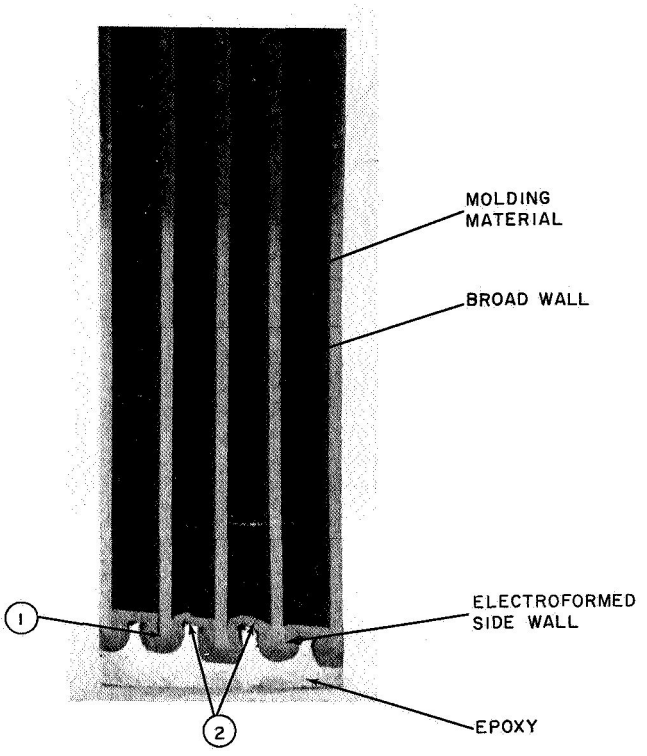

Figure 26. Detail of Electroformed Side Walls

An additional problem may arise because heat is needed for the particular molding compound used. Differences in the coefficients of thermal expansion and possible uneven heating could lead to stresses which would upset the precision of the horn array.

Alternative 1. - The problems found with the method described in the previous section may be corrected without any changes of the procedure outlined or the materials used. To prevent seepage between the fixture slots and the broad wall pieces, the slots in the fixture could be cut to make a tighter fit. This would require the precision machining of 100 slots such that seepage would be prevented yet the fixture could be easily removed. Such a task would be, in all likelihood, more difficult than producing the component parts for the lamination method.

The problem with the uneven side wall surface may be alleviated by using a suitable mold release agent on the surface of the fixture.

Alternative 2. - Both the seepage problem and the surface unevenness problem may be solved simultaneously. The temporary assembly may be done using a fixture similar to that shown in Figure 22 except that now the array would be made oversize or even rectangular to simplify the assembly fixture. The oversize assembly would then be machined to the required dimensions as shown in Figure 27 and the side wall would be electroplated as shown in Figure 28. An experimental model made in this

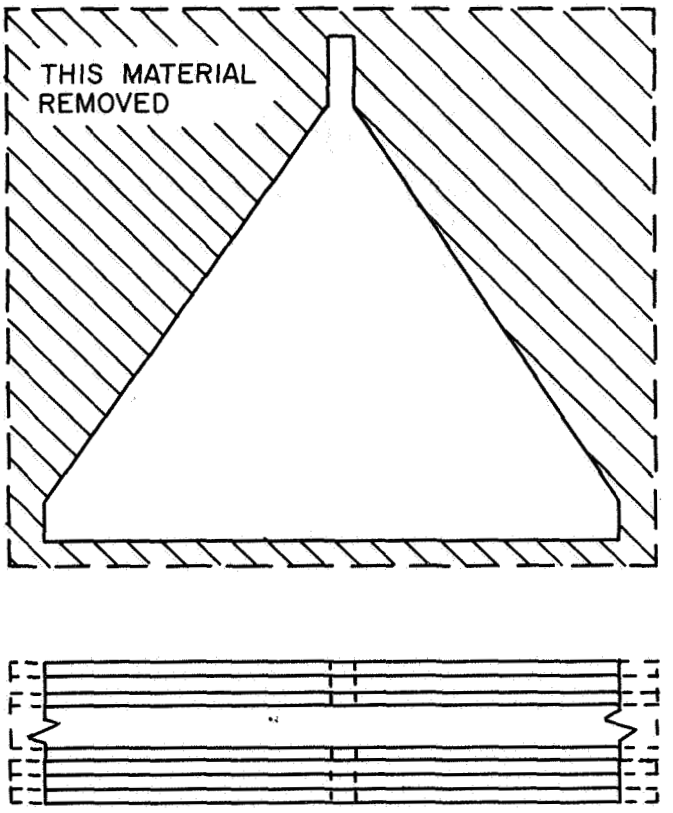

Figure 27. Oversize Assembly Machined to Final Dimensions

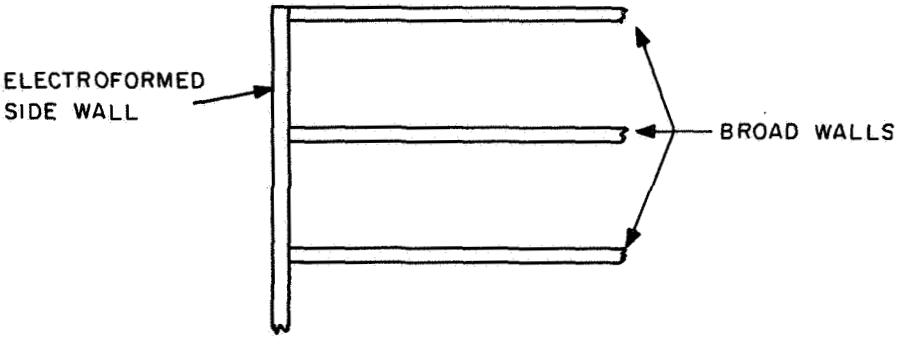

Figure 28. Side Wall Plated to Edges of Broad Walls

manner appears in Figure 29. This scheme yields a side wall which is as smooth as the molding compound can be machined. The joint between the broad wall and side wall will be a good deal weaker than the joint obtained from either of the two previous methods since the area of mechanical contact is only over the thickness of the broad wall. Also, the epoxy in the earlier methods supports the broad walls. The insertion of a lens into a horn which did not have quite sufficient clearance could result in breakage of the bond between the plated side wall and the top or bottom broad wall of that horn. The strength of the bond and the likelihood of the bond breaking requires further experimental study before anything more may be said about this approach.

Alternative 3. - The last method of electroforming the horn side walls to be discussed would use 50 individual spacers. The uniformity of the spacers could be most easily obtained by pre-casting them from the same mold. As before, the broad walls would be machined from sheet material and the spacers together with the broad wall pieces would be assembled in a fixture similar to that shown in Figure 22. The assembly would be clamped together and the fixture would be removed leaving the same kind of assembly shown in Figure 23a. The advantage here would be that the surfaces on which the side walls are formed would be absolutely smooth and the parts of the broad walls extending beyond the spacers would be clean. The spacers must be made of a material which is capable of supporting the compressive load of the assembly clamps. A likely candidate is polystyrene which can be removed with solvents. A soluble

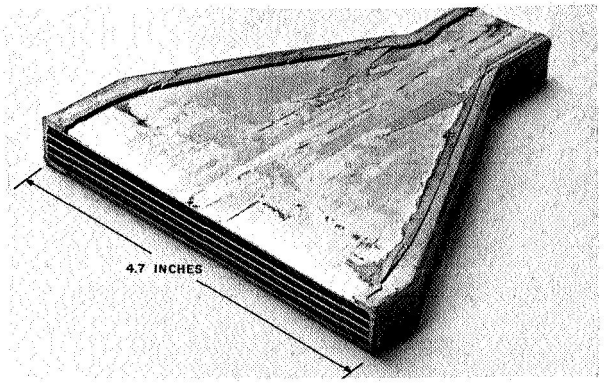

FRONT VIEW

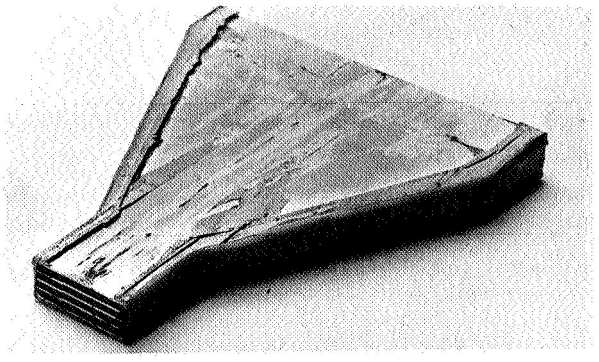

BACK VIEW

Figure 29. Electroformed 5-Horn Array

spacer material eliminates the problems caused by the necessity of heating the horn array to remove the spacers. The most evident problem is that the spacers must be precisely made and must indeed be uniform.

Choice of Approach. - Although each method of construction requires further investigation, Alternative 3 seems, at present, to be the best of the electroforming methods.

The lamination method of construction, however, must not be discarded as totally impractical at this time nor must any of the other electroforming methods. Only further experience will make a final decision possible.

Lenses

There are basically two methods of constructing the phase compensating lens required for the horn radiators and the power combiner. These are machining the lens from polystyrene sheet stock and casting the lens from bulk resin.

The lenses for the 16 GHz array were machined and were found to be satisfactory although costly to produce. The lenses for the 16 GHz array were machined in a profile tracing milling machine to insure uniformity and the same procedure could be followed for making the lenses for the 60 GHz array.

The impedance matching ridges on the lens surfaces are extremely thin and there was some concern about whether there would be any difficulty machining such a ridge in polystyrene. Figures 30 and 31 show a piece of polystyrene which was machined to the proper lens thickness and then had the longest and thinest anticipated matching

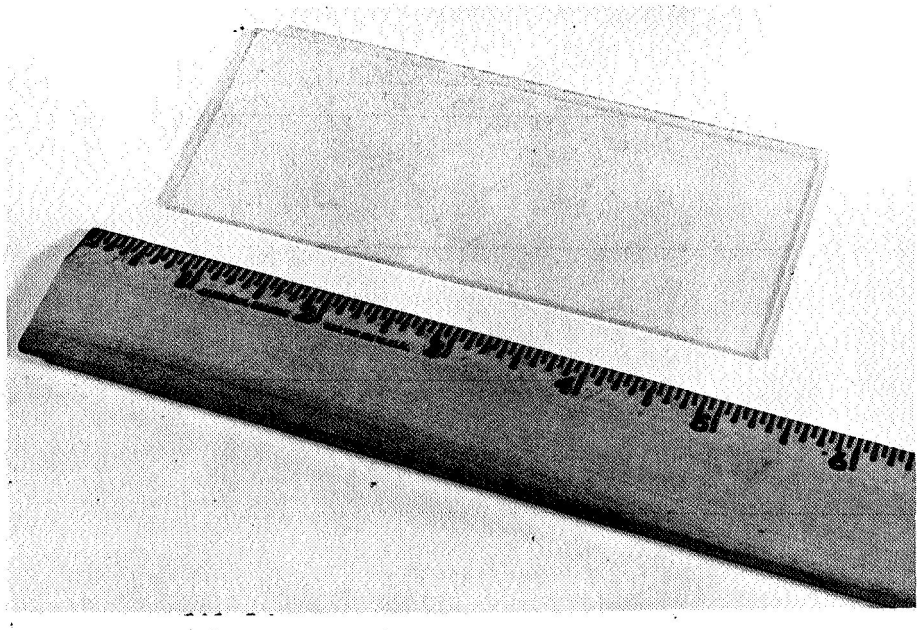

Figure 30. Machined Lens Blank

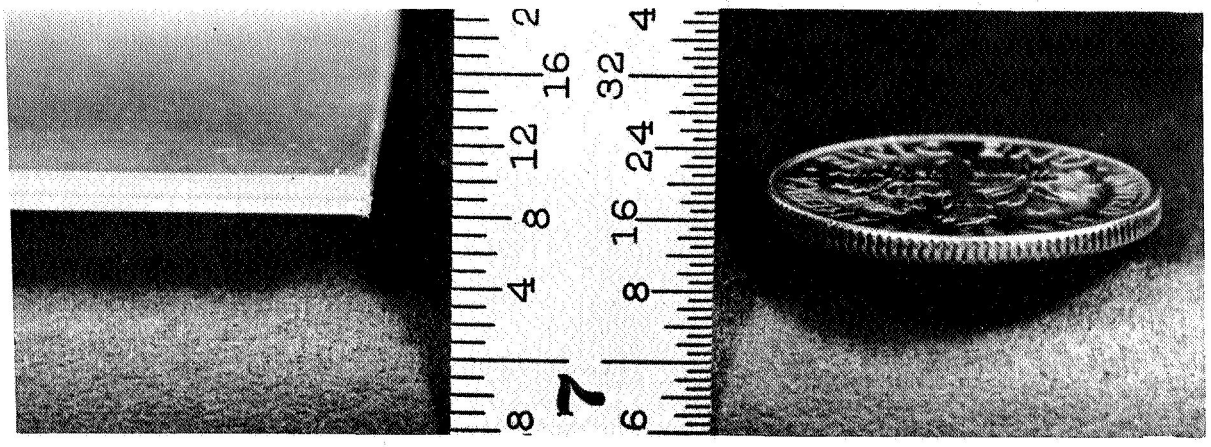

Figure 31. Machined Lens Matching Ridge

ridge machined into it. The ridge dimensions were held to within one thousandth of an inch and the ridge was not as fragile as had been expected. Maintaining a precision of bettern than 0.001 inch over the entire lens, however, is extremely difficult.

The lenses could be also made by casting them directly to their required dimensions. The use of a single precision mold each for the radiating element and power combiner lenses would insure uniformity of dimensions. This method would probably be less costly than the machining operation if the necessary casting facility is establishe

Power Combiner Horn

Two methods of manufacturing the power combiner horn present themselves. The first is identical to the procedure used at 16 GHz. The second is electroforming.

The 16 GHz power combiner horn was constructed by machining it directly into a block of metal as shown in Figure 32. This method is reasonably simple and it may be performed relatively easily with good precision. The main drawback is that the remaining wall thicknesses must be large enough to support themselves during the machining operations. This requirement adds extra weight.

The alternative approach is to electroform the power combiner horn using conventional electroforming techniques. The wall thickness here need only be great enough for the horn to support itself. The weight of such a horn could be easily adjusted to obtain an optimum strength and weight.

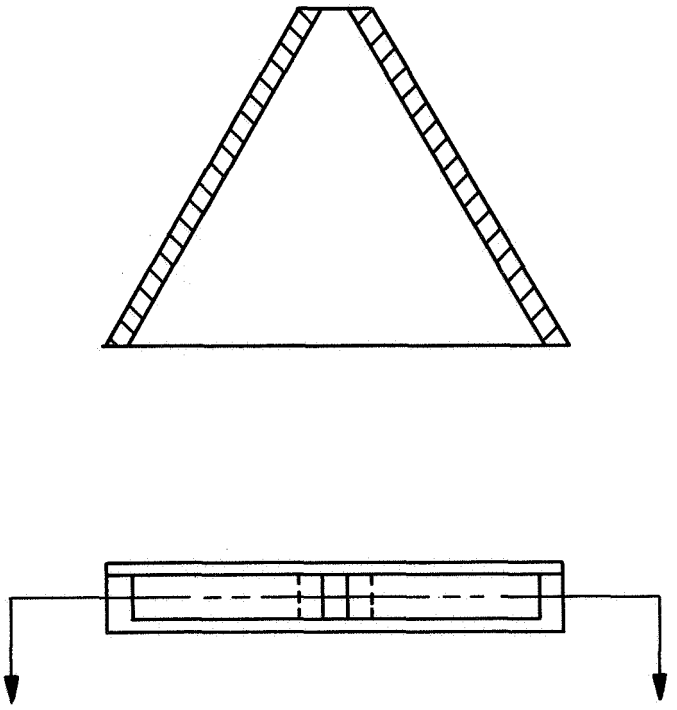

Figure 32. Power Combiner Horn Obtained by Machining

CONCLUSIONS

An initial design for the 60 GHz array is an almost direct scaling of the 16 GHz design. The array remains a very simple, low-loss device. Performance analyses have shown that if the 60 GHz phase shifter errors can be kept as small as has been obtained with C-band phase shifters, sidelobe levels do not increase intolerably and beam efficiencies greater than 90 percent may be expected.

Little has been reported in the literature about latching ferrite phase shifters at millimeter wavelengths and almost nothing has been reported at 60 GHz. An initial attempt in an experimental program to develop a 60 GHz latching ferrite phase shifter was unsuccessful but a second model is presently being constructed for evaluation. An analysis has shown that the best figure of merit of a 60 GHz phase shifter will be obtained by using a hexagonal-lattice ferrite material but this still must be experimentally verified. Therefore nothing conclusive may be said about the status of the 60 GHz latching ferrite phase shifter at the present time.

Electroforming methods seem to be the most promising ways of constructing the horn-array and power combiner horn. The uniformity of the dielectric lenses may best be obtained by casting them directly from bulk resin. The actual mechanical fabrication of the 60 GHz array, therefore, should present no insurmountable problems.

REFERENCES

1. C.E. Profera.: Phased Arrays for Meteorological Satellite. Interim Report prepared for NASA-ERC, June 1967, NASA-CR-86000.

2. C.E. Profera.: Phased Arrays for Meteorological Satellite. Interim Report prepared for NASA-ERC, June 1968, NASA-CR-86089.

3. T. Morita and S. B. Cohn.: Microwave Lens Matching by Simulated Quarter-Wave Transformers. Trans IRE, Vol. AP-3, pp 33-39, Jan. 1956.

4. P.H. Vartanian et al.: Propagation in Dielectric Slab Loaded Rectangular Waveguide. Trans IRE, Vol. MTT-6, pp 215-222, April 1958.

5. Richard A. Stern and John P. Agrios.: A Fast Millimeter Ferrite Latching Switch. PGMTT Symposium Digest, p. 219 (1966).

6. E. Wantuch, J.E. Degenford and L.R. Whicker.: Modified Ferrites with High Saturation Magnetization and Improved Hysteresis Properties. Journal of Applied Physics, Vol. 39, Number 2, p. 723, Feb. 1968.

7. S. Berger, Private correspondence.

8. J.L. Allen.: Some Extensions of the Theory of Random Error Effects on Array Patterns. Phased Array Radar Studies, Chap. III, 1 July 1960 to 1 July 1961, Lincoln Laboratory, TR-236.

9. C.J. Miller.: Minimizing the Effects of Phase Quantization Errors in an Electronically Scanned Array. Proceedings of Symposium on Electronically Scanned Array Techniques and Applications, RADC TDR 64-225, Vol. 1, July 1964.

New Technology Appendix

After a diligent review of the work performed under this contract, no new innovation, discovery, improvement or invention was made.